Safe speeds for a heavy articulated vehicle when passing a floating bridge tower under crosswind

Results in Engineering 23 (2024) 102496

Contents lists available at ScienceDirect

Results in Engineering

journal homepage: www.sciencedirect.com/journal/results-in-engineering

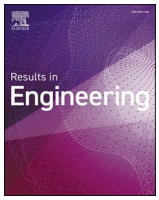

Safe speeds for a heavy articulated vehicle when passing a floating bridge tower under crosswind

Dragan Sekulic [a,*], Alexey Vdovin [a], Bengt Jacobson [a], Simone Sebben [a], Stian Moe Johannesen [b]

[a] Chalmers University of Technology, Gothenburg, Sweden
[b] The Norwegian Public Road Administration, Oslo, Norway

ARTICLE INFO

Keywords:
Bjørnafjorden
Aerodynamic loads
Rollover risk
Traffic lane departure
Tractor-semitrailer
Vehicle modelling
Simulation

ABSTRACT

This paper recommends safe speeds for a heavy articulated vehicle when passing by Bjørnafjorden floating bridge tower under two constant crosswind speeds (65 km/h and 100 km/h). The analysis is based on the tractor-semitrailer (TS) model with fifth-wheel (FW) coupling in roll and free in yaw. Comparison of safe speeds assessments has been made with two TS models differ in FW coupling. Aerodynamic forces and moments for TS models as function of their position relative to the bridge tower and time were computed using Computational Fluid Dynamics (CFD) simulations. For TS model coupled in roll and free in yaw, no rollover risk is noticeable for both crosswind excitations. For TS model free in roll and in yaw, roll-over risk is noticeable at lower vehicle velocities (at 36 km/h and 54 km/h). TS with rigid connection in FW stays in the traffic lane for every considered vehicle velocity. TS model which is roll and yaw moment free in the FW overestimates rollover risk assessment at lower vehicle velocities. TS model with rigid connection in the FW underestimates traffic lane departure assessment at higher vehicle velocity. Appropriate mathematical modelling of a heavy articulated vehicle that considers tractor and semitrailer units as two separate bodies coupled in roll and free in yaw is of importance for accurately assessing safe speeds when a vehicle passing by the bridge tower.

1. Introduction

Norway's largest transport project, the *Coastal Highway Route E39*, aims to significantly reduce travel time on the west coast. There are eight fjords being operated by ferries on this route (Fig. 1). Various types of high-tech constructions will replace ferries across huge fjords (e.g. floating and suspension bridges, floating and road tunnels, [1]). Some of the fjords are challenging to cross since of their width and depth dimensions. One of the proposed solutions for crossing of Bjørnafjorden (approximately 5 km wide and 550 m deep) is straight floating bridge concept (Fig. 1b). On route E39 the typical driving speed for an articulated vehicle is 80 km/h and for a passenger car is 110 km/h. Design driving speed on Bjørnafjorden floating bridge is 110 km/h [1].

Floating bridge is extreme construction exposed to the winds and waves from the North Sea during inclement weather condition. Traveling over the bridge might be unsafe during harsh weather conditions. Closing the bridge for traffic will increase the travel time on the route and driving costs for the road users. The straight bridge is stiffened laterally by mooring lines connecting bridge pontoons with the seabed at four points (Fig. 1b) to prevent its excessive motion. At the south part, bridge deck is fixed by the tower (Fig. 1b). Tower is 12 m in length and placed on the higher part of the bridge on distance of 450 m from the beginning (from axis O, Fig. 2). When running by the tower, a vehicle goes through two phases. In the first phase, a vehicle is shielded by the tower, and the intensity of the crosswind is significantly reduced. In the second phase, the vehicle leaves the tower, and the intensity of the crosswind load on a vehicle sharply increases. Such changes in crosswind load are demanding for a driver and require his quick reactions to prevent the vehicle from overturning or departing the traffic lane [2]. This is specifically case for the unloaded high-sided heavy vehicle (e.g. bus, TS). There is few evidence about traffic accidents happened on long span bridges caused by strong crosswind gust. Seven high-sided road vehicles were overturned on the Humen suspension bridge in China due to intensive crosswind gust on August 11, 2004 [2]. A similar accident occurred in 2005 with road vehicles traveling on the Minjiang cable-stayed bridge in China [2,3].

The aerodynamic forces acting on a stationary and moving vehicle behind the bridge tower have been studied numerically using

* Corresponding author.
E-mail addresses: d.sekulic@sf.bg.ac.rs (D. Sekulic), alexey.vdovin@chalmers.se (A. Vdovin), bengt.jacobson@chalmers.se (B. Jacobson), simone.sebben@chalmers.se (S. Sebben), stian.moe.johannesen@vegvesen.no (S.M. Johannesen).

https://doi.org/10.1016/j.rineng.2024.102496
Received 15 April 2024; Received in revised form 14 June 2024; Accepted 1 July 2024
Available online 3 July 2024

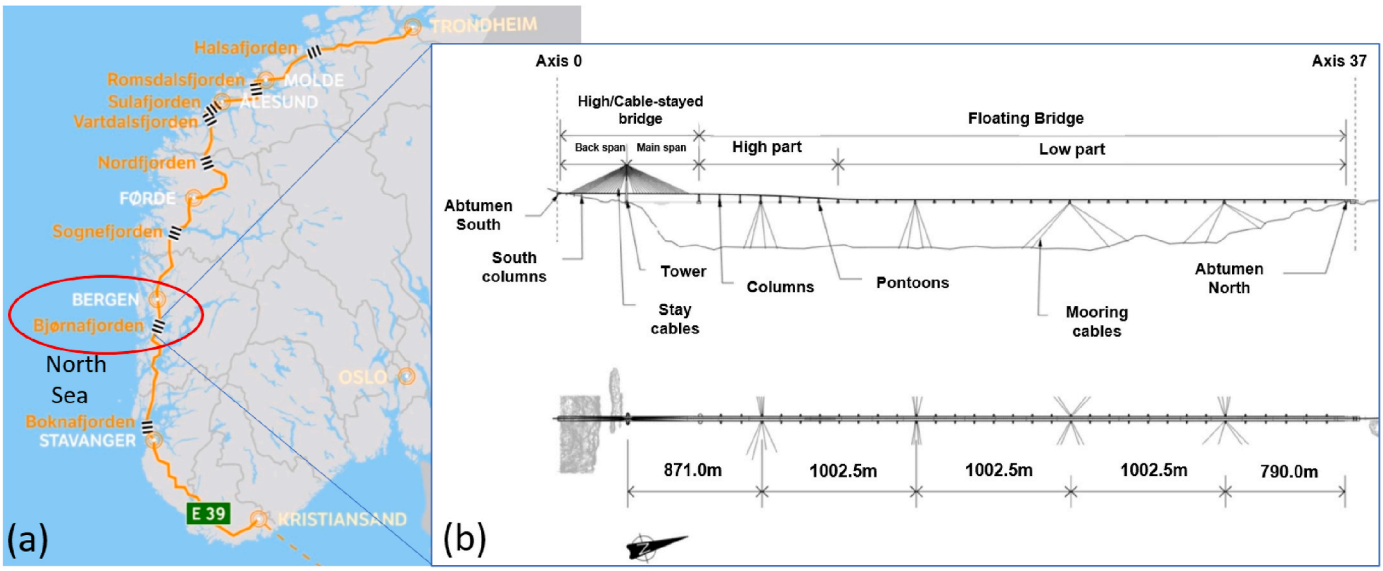

Fig. 1. Route E39 a) Bjørnafjorden; b) straight floating bridge concept [1].

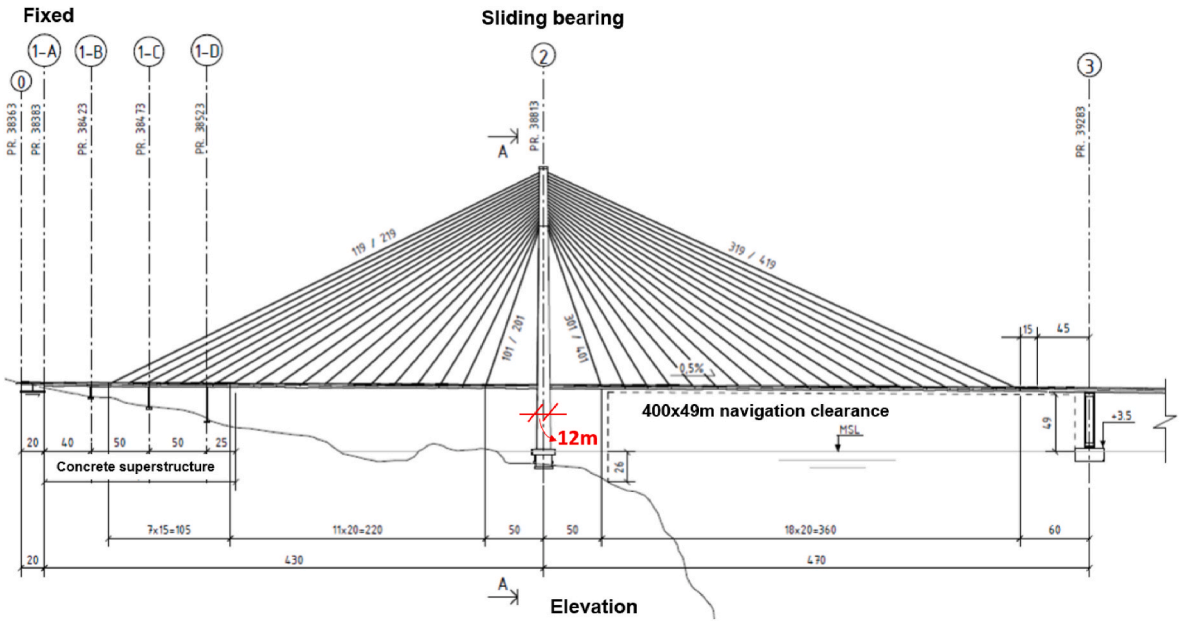

Fig. 2. Bridge tower position on the floating bridge deck and characteristic dimensions [1].

computational fluid dynamics (CFD) software [4]. Study showed that side force coefficients of the moving vehicle are lower than those of the stationary one for the same vehicle positions. Influence of the wind barriers installed around bridge tower on aerodynamic loads affecting a long vehicle had been investigating in Ref. [5]. Aerodynamic forces and moments had been measured in the wind tunnel tests on a 1:40 TS scale model. In the tests vehicle model was stationary and placed at different location relative to the bridge tower. Also, vehicle length was longer than the tower width. Study showed that aerodynamic loads (e.g. wind side force and rolling moment) increased on the stationary vehicle centred behind the tower. In the case of the barriers present, wind side forces could change sign when the vehicle is placed behind the tower. Investigations of the vehicle-driver behaviour when passing by the tower of long span cable-stayed bridge under the crosswind of 15 m/s mean speed and two vehicle speeds (80 km/h and 90 km/h) had been done in Ref. [2]. Nonlinear one-unit heavy vehicle model with 6 Degrees of Freedom (DOF) (i.e. no articulation angle DOF considered) and with two axles had been defined. This study showed that unlike the vertical and pitch motions, the vehicle roll, and lateral motions are significantly influenced by the tower. No rollover risk for the one-unit vehicle has been noticed in this study.

There are vehicle mathematical models of different levels of complexity used for the investigations of their dynamics behaviour on long span bridges [2,6,7,8]. Complexity of a vehicle mathematical model depends on an aim of an analysis. Simplified one-rigid unit heavy vehicle model with 6 DOF does not consider suspension system elements when analysing vehicle rollover risk [2]. High-sided vehicle model of 11 DOF incorporates spring-damper elements for vehicle suspension system and tyres, and it was used for comfort and safety analysis on slender arch bridge under turbulent wind [8]. It was assumed that the vehicle run

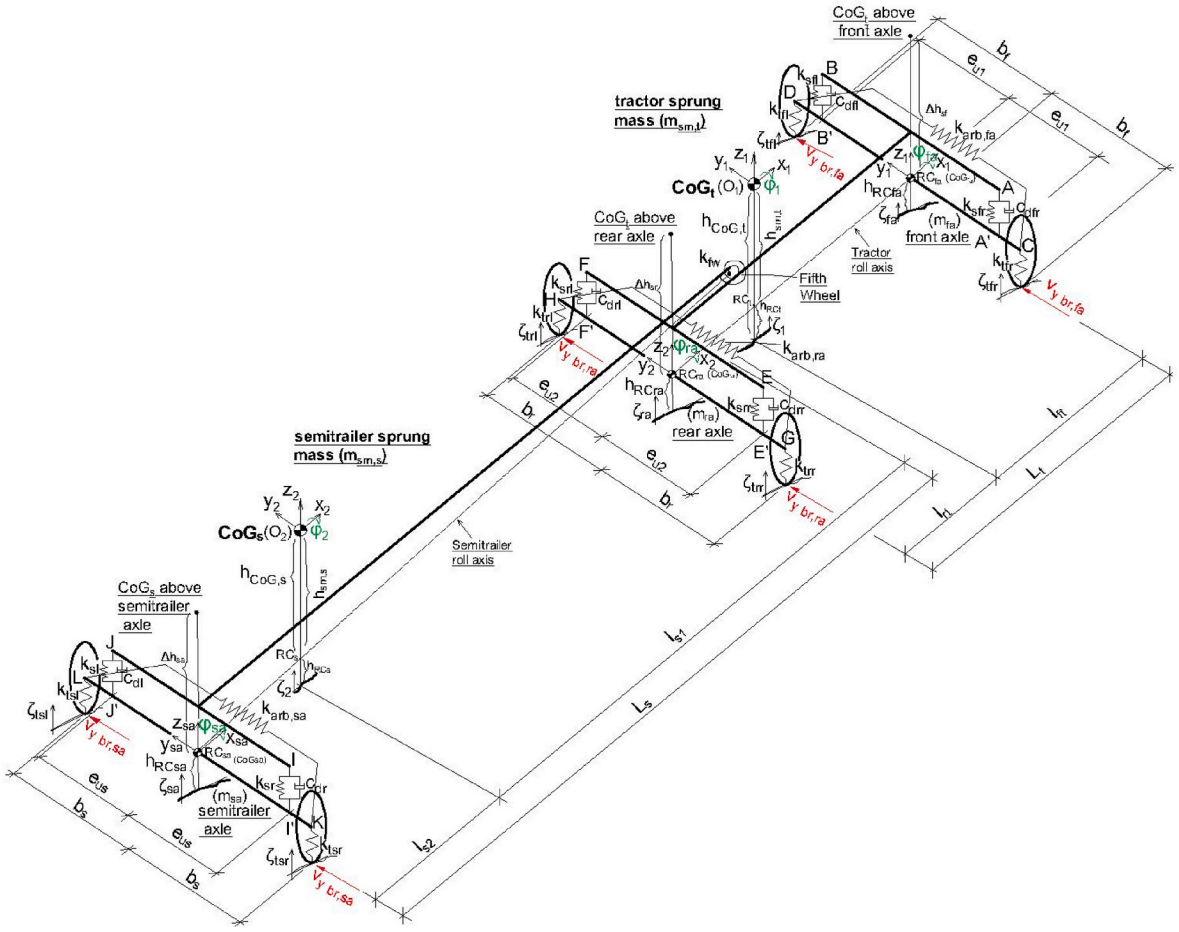

Fig. 3. TS model with roll-stiffness (k_{fw}) in the FW.

along straight line and driver model was not included. TS model of 19 DOF had been defined in Ref. [7]. This model considers tractor and semitrailer units separately and three rigid axles and was used for ride comfort analysis on long-span bridge under crosswind. It was assumed that the vehicle moved along straight line at constant velocity and no driver model was included. Unlike the previously mentioned heavy vehicle models, TS model of 9 DOF is convenient for the analysis of its lateral stability on floating bridges [6]. It considers tractor and semitrailer units separately (i.e. articulation point included), three rigid axles, suspension system and tyres together with the driver model.

The main objective of this work is to recommend safe speeds for a heavy articulated vehicle passing by the floating bridge tower under the influence of the different constant crosswinds' speeds. The second objective of this work is to investigate the influence of the roll-stiffness in the articulated point on safe speeds assessment. For these investigations, modified two units TS model with 9 DOF, which baseline version was previously defined in Ref. [6], had been used. Modified TS model considers the roll-stiffness in the FW. The third objective of this study is to analyse the importance of articulation angle DOF in TS model and its influence on safe speeds assessment. For this analyse one rigid TS model with 7 DOF was defined based on TS model in Ref. [6]. In our investigations we employed simulation method. Vehicle modelling and all simulations have been done in MATLAB/Simulink software.

2. Description of the tractor semitrailer models

In this paper two modified versions of the baseline TS model with 9 DOF previously defined in Ref. [6] have been used. TS model consists of two units (tractor and semitrailer) connected at articulated point by FW coupling. There are two alternatives for FW modelling: it could be modelled with the spring of the rotational stiffness k_{fw} in the roll DOF (Fig. 3) or it could be modelled to be roll rigid (Fig. 4).

When defining TS models, all assumptions from Ref. [6] have been applied, except one which state that the articulation joint is free of a roll moment.

2.1. TS model with FW coupling in roll with the rotational stiffness k_{fw}

Fig. 3 presents modified TS model which considers FW coupling in roll (k_{fw}) unlike the basic TS model from Ref. [6]. Modified TS model considers tractor unit sprung mass ($m_{sm,t}$), semtrailer unit sprung mass ($m_{sm,s}$), tractor fron axle (m_{fa}), tractor rear axle (m_{ra}) and semitrailer axle (m_{sa}). Suspension systems on the left and on the right side of each rigid axle are modelled with the spring and the damper elements. Suspension systems also consider anti-roll bar on each axle. The tyre on every axle is modelled with the spring element. Spring stiffness coefficients, damping coefficient and anti-roll bar coefficients are given in Appendix (Table 1). The influence of the roll-stiffness in the FW on the vehicle responses and the safe speeds assessment is presented in section 4.

Modified TS model was defined by Lagrangian method including kinetic energy, potential energy, and dissipative energy of the system. Kinetic and dissipative energies of the system take the same form as for the baseline TS model described by Eqs. (13) and (17) in Ref. [6]. Potential energy includes spring deformation in the FW unlike the baseline TS model, given by Eq. (1)

$$V_{pot.} = \frac{1}{2}k_{sfl}2e_{u1}^2(\phi_1 - \phi_{fa})^2 + \frac{1}{2}k_{srl}2e_{u2}^2(\phi_1 - \phi_{ra})^2 + \frac{1}{2}k_{sl}2e_{us}^2(\phi_2 - \phi_{sa})^2 + \frac{1}{2}k_{tfl}\left((\zeta_{fa} + b_f\phi_{fa} - \zeta_{tfl})^2 + (\zeta_{fa} - b_f\phi_{fa} - \zeta_{tfr})^2\right) + \frac{1}{2}k_{trl}\left((\zeta_{ra} + b_r\phi_{ra} - \zeta_{trl})^2 + (\zeta_{ra} - b_r\phi_{ra} - \zeta_{trr})^2\right) + \frac{1}{2}k_{tsl}\left((\zeta_{sa} + b_s\phi_{sa} - \zeta_{tsl})^2 + (\zeta_{sa} - b_s\phi_{sa} - \zeta_{tsr})^2\right) + \frac{1}{2}k_{arb,fa}(\phi_1 - \phi_{fa})^2 + \frac{1}{2}k_{arb,ra}(\phi_1 - \phi_{ra})^2 + \frac{1}{2}k_{arb,sa}(\phi_2 - \phi_{sa})^2 - \frac{1}{2}m_{sm,t}gh_{sm,t}{\phi_1}^2 - \frac{1}{2}m_{sm,s}gh_{sm,s}{\phi_2}^2 + \frac{1}{2}k_{fw}(\phi_1 - \phi_2)^2 \quad (1)$$

Detail description of the generalized forces definition could be found in section 2.1.2.4 in Ref. [6]. The notations in Fig. 3 and in Eq. (1) and their values are given in Appendix (Table 1). Available literature was used to obtain the typical values for TS vehicle [9–16,17]. Method to introduce wind excitations on the detailed TS vehicle model from Adams database for the investigation of its dynamic behaviour on Bjørnafjorden floating bridge has been presented in Ref. [16]. Analysis considered random varying wind velocity signal acting on the TS model along the whole length of the bridge. This work considers wind disturbance caused the bridge tower which is a single strong transient excitation unlike the wind excitation from Ref. [16].

2.2. TS model with FW rigid in roll and yaw

TS model with the rigid connection (rigid in roll and yaw) in the FW was defined to investigate its influence on the vehicle responses (e.g. traffic lane departure, section 4.4.2) and the safe speeds assessment. Defined one rigid body (one roll-stiff unit) TS model has 7 DOF in total, and 2 DOF less than baseline TS model (no articulation angle and no relative roll-motion between vehicle units). The vehicle out-of-road-plane DOFs are roll motions of the vehicle sprung mass, first, second and third axles (ϕ, ϕ_{fa}, ϕ_{sa}, and ϕ_{ta}), (Fig. 4). The vehicle in-road-plane DOFs are the longitudinal, lateral and yaw motions (X_1, Y_1, ψ), (Fig. 5a). The notations in Fig. 4 and their values are given in Appendix (Table 1).

Mathematical model was built on Lagrangian method, Eq. (2)

$$\frac{d}{dt}\frac{\partial T_{tot.}}{\partial \dot{q}_i} - \frac{\partial T_{tot.}}{\partial q_i} + \frac{\partial V_{pot.}}{\partial q_i} + \frac{\partial D_{dis.}}{\partial q_i} = Q_i, i = 1, \ldots, n; \quad (2)$$

where $T_{tot.}$, $V_{pot.}$ and $D_{dis.}$ are the kinetic, potential, and dissipative energy of the system, respectively; q_i, $\dot{q}_i$, Q_i refers to generalized coordinates, velocities, and forces; and n are all generalized coordinates of the system.

The generalized coordinates for the one rigid body TS model are

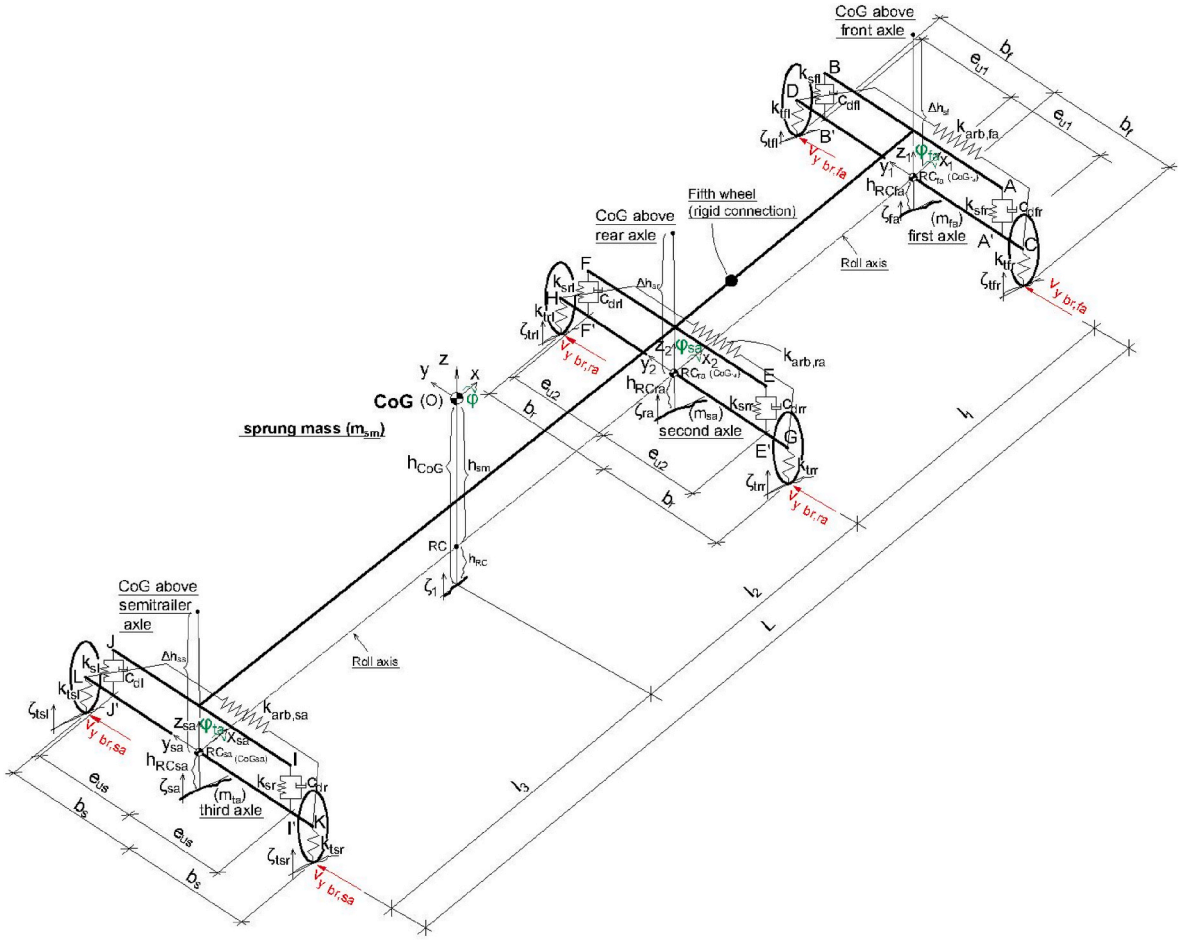

Fig. 4. One rigid body TS model with three axles.

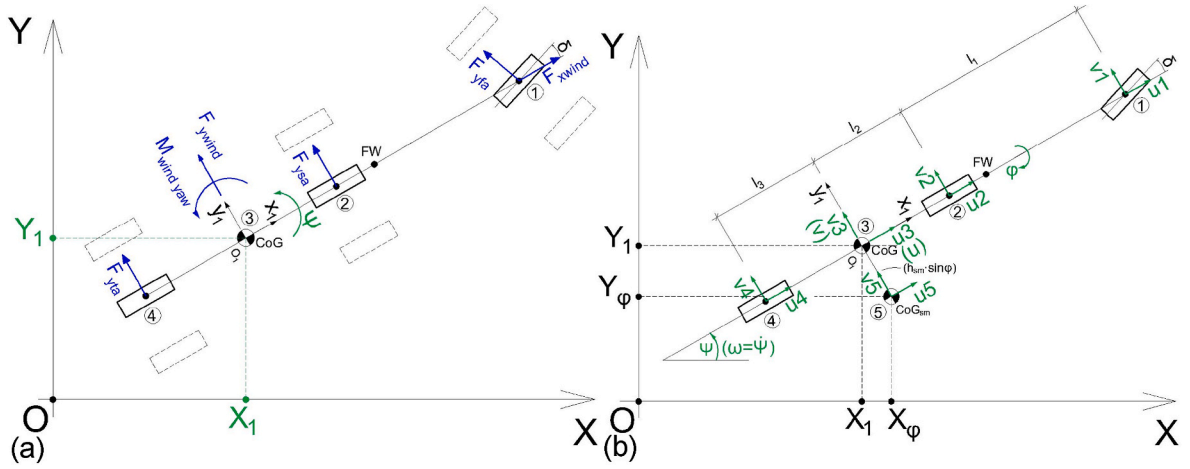

Fig. 5. Vehicle a) in-plane motion and external forces/moments (view from above), b) velocities of rigid body CoGs.

presented by Eq. (3)

$$q = [X_1;\ Y_1;\ \psi;\ \phi;\ \phi_{fa};\ \phi_{sa};\ \phi_{ta}] \tag{3}$$

Lagrangian equations were derived using MATLAB symbolic toolbox and using the equations in sections 2.2.1 - 2.2.4. The result was used in a dynamic model in Simulink, where each generalized coordinate was represented by a state variable using a Simulink model (an integrator block).

2.2.1. Kinetic energy

Total kinetic energy of the system is given by Eq. (4)

$$T_{tot.} = T_{in-road-plane} + T_{out-of-road-plane} \tag{4}$$

where $T_{in\text{-}road\text{-}plane}$ is kinetic energy due to in-plane motion; $T_{out\text{-}of\text{-}road\text{-}plane}$ is kinetic energy due to out-of-plane motion. The longitudinal and lateral velocities of the vehicle rigid bodies Centre of Gravity (CoG) (Points 1–5, Fig. 5b) are given by Eqs. (5)–(9).

- Point 1, (first axle),

$$\begin{aligned} u1 &= u \\ v1 &= v + (l_1 + l_2)\omega \end{aligned} \tag{5}$$

- Point 2, (second axle),

$$\begin{aligned} u2 &= u \\ v2 &= v + l_2\omega \end{aligned} \tag{6}$$

- Point 3, (CoG of the vehicle),

$$\begin{aligned} u3 &= u \\ v3 &= v \end{aligned} \tag{7}$$

- Point 4, (third axle),

$$\begin{aligned} u4 &= u \\ v4 &= v - l_3\omega \end{aligned} \tag{8}$$

- Point 5, (CoG of the vehicle sprung mass),

$$\begin{aligned} u5 &= u + h_{sm}\omega \sin\phi \\ v5 &= v - h_{sm}\dot{\phi}\cos\phi \end{aligned} \tag{9}$$

The total kinetic energy of the system is given by Eq. (10) and used in Eq. (2)

$$\begin{aligned} T_{tot.} = {} & \frac{1}{2}J\dot{\psi}^2 + \frac{1}{2}m_{fa}(u1^2 + v1^2) + \frac{1}{2}m_{sa}(u2^2 + v2^2) + \frac{1}{2}m_{ta}(u4^2 + v4^2) \\ & + \frac{1}{2}m_{sm}(u5^2 + v5^2) + \frac{1}{2}J_{fa}\dot{\phi}_{fa}^2 + \frac{1}{2}J_{sa}\dot{\phi}_{sa}^2 + \frac{1}{2}J_{ta}\dot{\phi}_{ta}^2 + \frac{1}{2}J_{sm}\dot{\phi}^2 \end{aligned} \tag{10}$$

2.2.2. Potential energy

Potential energy of the system takes into account roll motion-induced height change of the vehicle sprung mass CoG, deformation of anti-roll bar on every axle, deformation of air springs in the suspension system on every axle and radial deformation of tires (Fig. 4). Potential energy is defined by Eq. (11), and used in Eq. (2)

$$\begin{aligned} V_{pot.} = {} & \frac{1}{2}k_{sfl}2e_{u1}^2(\phi - \phi_{fa})^2 + \frac{1}{2}k_{sri}2e_{u2}^2(\phi - \phi_{sa})^2 + \frac{1}{2}k_{sl}2e_{us}^2(\phi - \phi_{ta})^2 + \frac{1}{2}k_{tfl}\left((\zeta_{fa} + b_f\phi_{fa} - \zeta_{tfl})^2 + (\zeta_{fa} - b_f\phi_{fa} - \zeta_{tfr})^2\right) + \frac{1}{2}k_{trl}\left((\zeta_{ra} + b_r\phi_{sa} - \zeta_{trl})^2\right. \\ & \left. + (\zeta_{ra} - b_r\phi_{sa} - \zeta_{trr})^2\right) + \frac{1}{2}k_{tsl}\left((\zeta_{sa} + b_s\phi_{ta} - \zeta_{tsl})^2 + (\zeta_{sa} - b_s\phi_{ta} - \zeta_{tsr})^2\right) + \frac{1}{2}k_{arb,fa}(\phi - \phi_{fa})^2 + \frac{1}{2}k_{arb,ra}(\phi - \phi_{sa})^2 + \frac{1}{2}k_{arb,sa}(\phi - \phi_{ta})^2 - \frac{1}{2}m_{sm}gh_{sm}\phi^2 \end{aligned} \tag{11}$$

2.2.3. Dissipative energy

Viscous dampers in the vehicle suspension system cause the dissipative energy. This energy could be expressed by Eq. (12), and used in Eq. (2)

$$D_{dis.} = \frac{1}{2}c_{dfl}2e_{u1}^2(\dot{\phi} - \dot{\phi_{fa}})^2 + \frac{1}{2}c_{drl}2e_{u2}^2(\dot{\phi} - \dot{\phi_{sa}})^2 + \frac{1}{2}c_{dl}2e_{us}^2(\dot{\phi} - \dot{\phi_{ta}})^2 \tag{12}$$

2.2.4. Generalized forces

Generalized forces (Q_i) are the external (tire and wind) forces (Fig. 5a). They are expressed as functions of the velocity vectors (Eqs. (5)–(9)). Details are found in section 2.1.2.4 in Ref. [6].

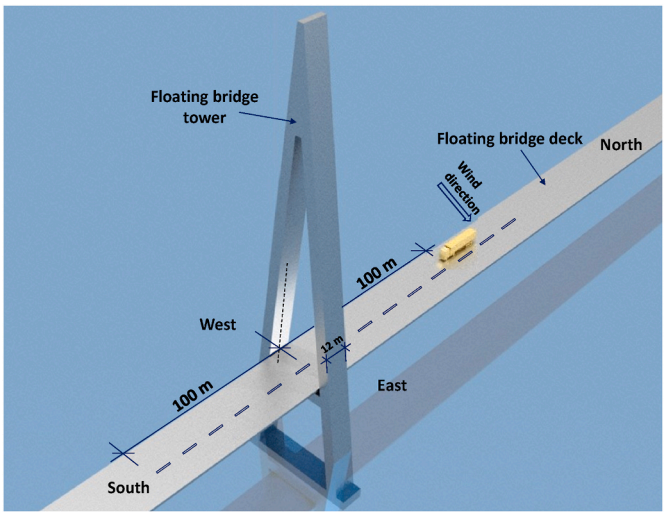

Fig. 6. TS model on the floating bridge deck for CFD simulations.

2.3. Aerodynamic loads computation

In earlier studies [6,18] of the traffic over this bridge, the influence from other objects, such as the tower, has not been included. Those studies only had vehicle velocity changing. Hence, it was possible to convert the aerodynamic forces into non-dimensional coefficients to simplify the comparisons of different cases and recalculate the aerodynamic forces for the cases that were not simulated. However, in this study both wind and vehicle velocities vary, and choosing a single reference velocity for different cases can not be performed. In addition, it means that all presented cases with different vehicle and wind velocity need to be simulated without an advantage provided by using aerodynamic coefficients. Consequently, in this study the aerodynamic forces are presented as they are. Additionally, other numerical studies showed the importance of having a dynamically moving mesh for the vehicle passing a tower [4]. Therefore, this study takes a similar approach, with a stationary mesh region surrounding the bridge structures constantly exchanging the necessary parameters to a moving overset mesh region containing a vehicle that dynamically moves.

CFD simulations have been extensively used for calculation of aerodynamic loads acting on a vehicle [19,20]. Aerodynamic forces and moments for both TS models as function of their position relative to the bridge tower and time were computed for two constant crosswind

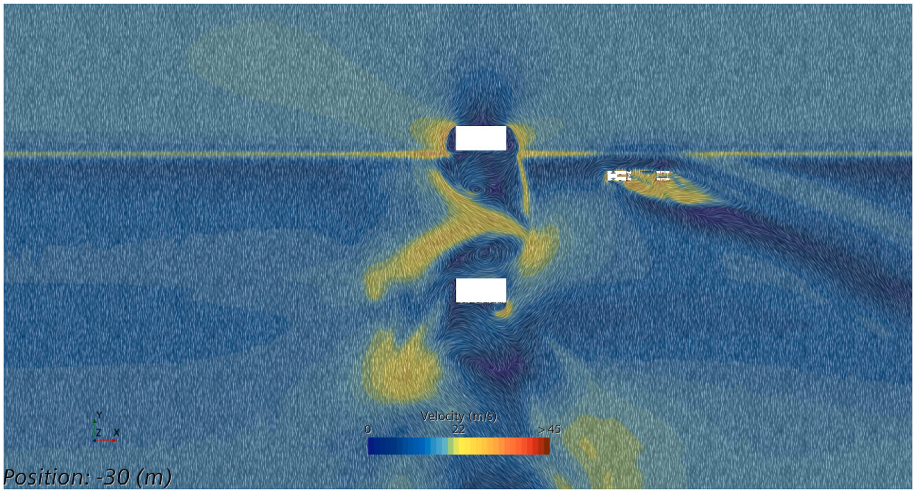

Fig. 7. Vector plot of the velocity field showing the wheel centre hight horizontal cutting plane.

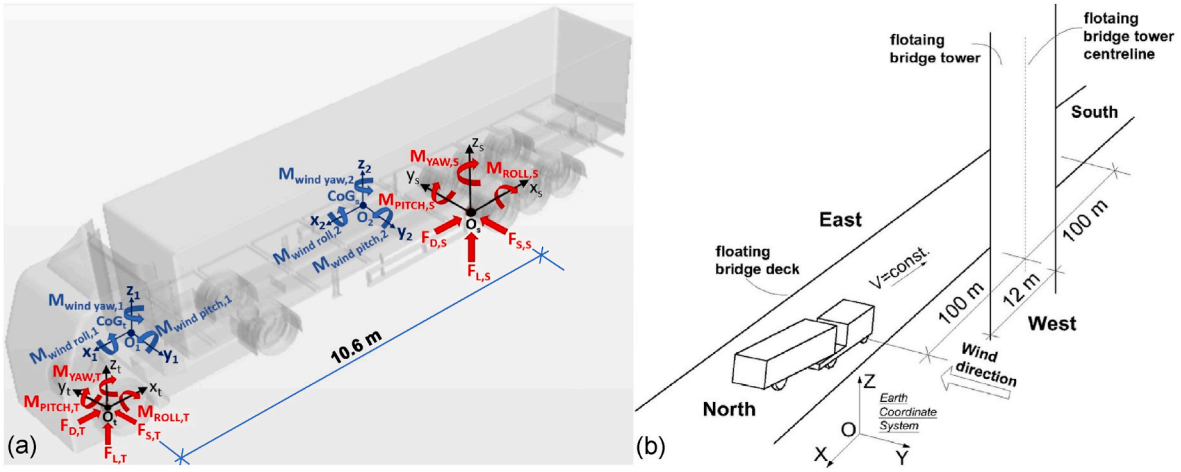

Fig. 8. TS model with articulation angle DOF a) with reference coordinate systems (ISO 4130) and sign convention; b) characteristic distances relative to floating bridge tower.

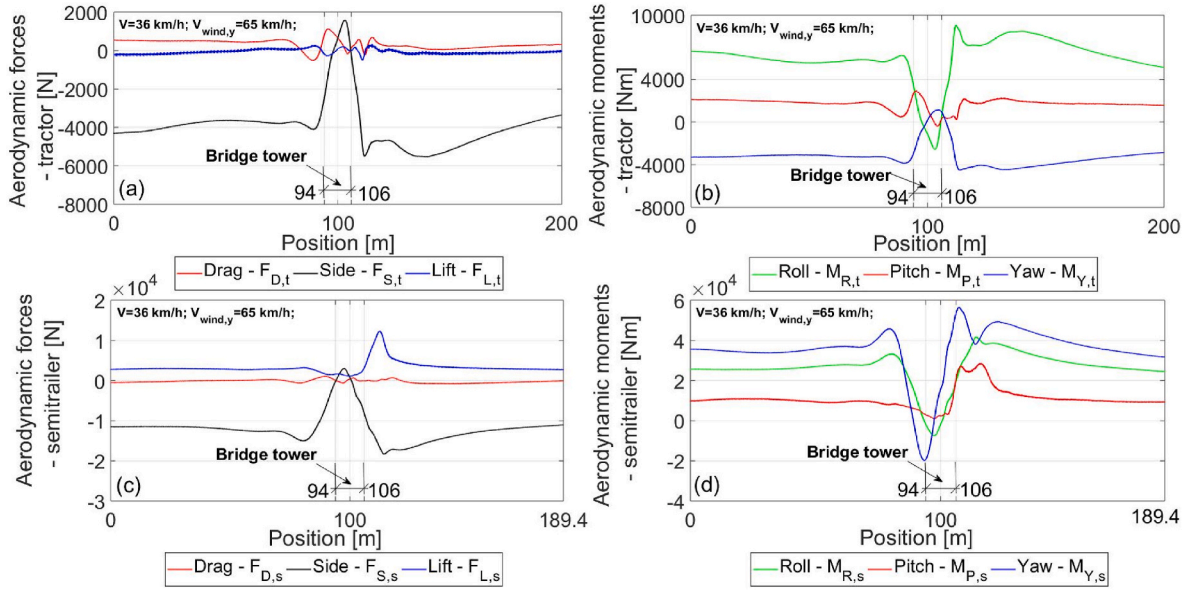

Fig. 9. Aerodynamic a) forces for tractor unit; b) moments for tractor unit; c) forces for semitrailer unit; and d) moments for semitrailer unit, for the vehicle velocity of 36 km/h and the crosswind speed of 65 km/h.

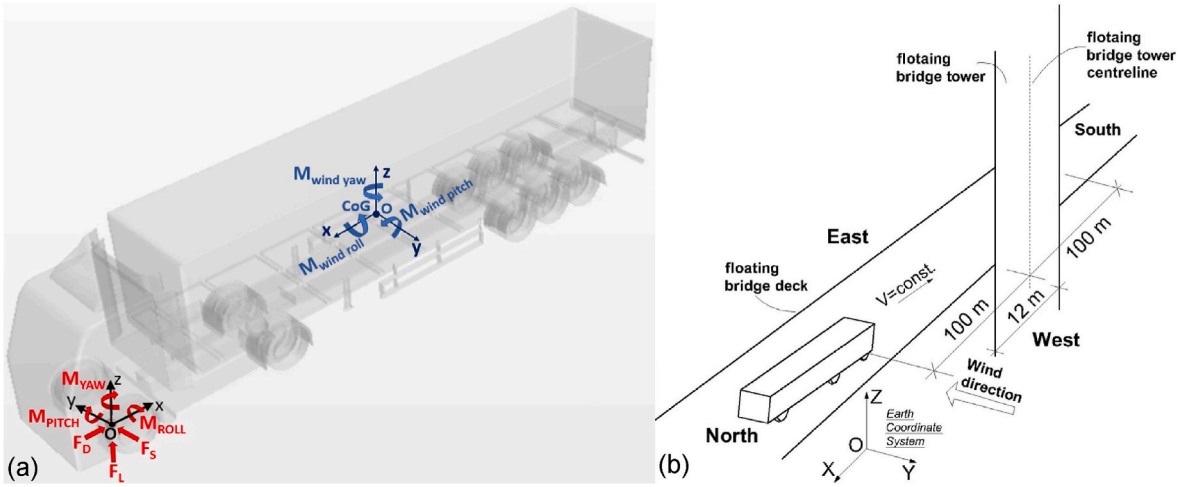

Fig. 10. TS model with the rigid connection in the FW a) with reference coordinate system (ISO 4130) and sign convention; b) characteristic distances relative to floating bridge tower.

speeds of 65 km/h and 100 km/h using CFD simulations. Overview of the CFD simulation setup is presented in Fig. 6. Vehicle runs in the North-South direction placed in the nearest traffic lane to the bridge tower since aerodynamic forces and moments are of the large values for this lane [3,21,22]. TS changes its position relative to the tower on the distance of one hundred meters before and after the bridge tower.

Firstly, the flow-field around the bridge structures and the TS positioned 120 m away from the tower is solved using a steady-state Reynolds-Averaged Navier-Stokes approach with an ideal gas model for air and realizable k-epsilon model for turbulence. This solution is then used as a starting condition for the Unsteady-RANS simulation when the overset mesh approach is taken to model the vehicle movement through the tower wake. An example of the CFD results can be seen in Fig. 7, where vector plot of the velocity field showing the wheel centre hight horizontal cutting plane can be seen. The vortex structures around the towers and the wake behind the TS can clearly be observed as well as the flow acceleration around the bridge deck.

For the simulation domain only 100 m before and after the bridge tower are considered as on this distance the effect of bridge tower wake become insignificant.

Fig. 8a shows TS model with two units used in CFD simulations. Two ISO 4130 reference coordinate systems were placed in the ground plane for obtaining aerodynamic forces and moments for both vehicle units. Red arrows point out positive direction according to sign convention. Two vehicle fixed coordinate systems (ISO 8855) are attached to vehicle units CoGs. Aerodynamic forces and moments were transformed into the vehicle fixed coordinate systems when performing simulations.

Fig. 9 shows aerodynamic forces and moments as a function of distance for the tractor and semitrailer units for the vehicle velocity of 36 km/h and the crosswind speed of 65 km/h. Side forces and rolling moments on both units decrease and then increase when TS passing by the tower. Considerable change is noticed for yawing moment on semitrailer unit (Fig. 9d). Yawing moment change its sign when semitrailer is shielded by the tower (Fig. 9d).

Fig. 10a shows TS model with one unit used in CFD simulations. Origin of the ISO 4130 reference coordinate system (point O) is at the intersection point of the front axle projection on the ground and the mid-track line. Red arrows point out positive direction according to the sign

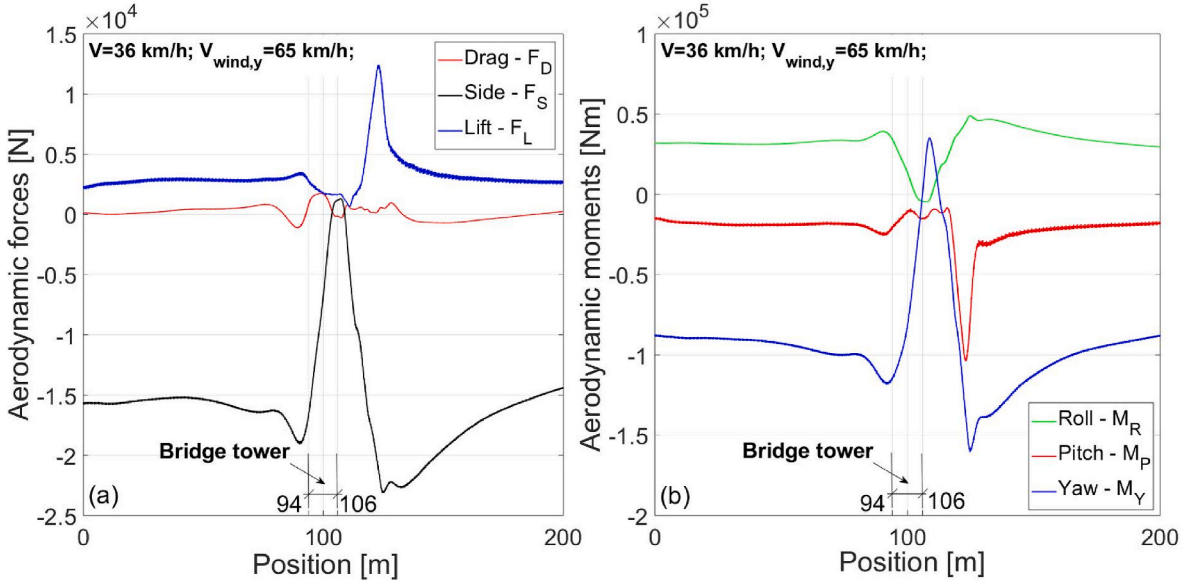

Fig. 11. Aerodynamic loads on the one rigid body TS model a) forces; b) moments, for the vehicle velocity of 36 km/h and the crosswind speed of 65 km/h.

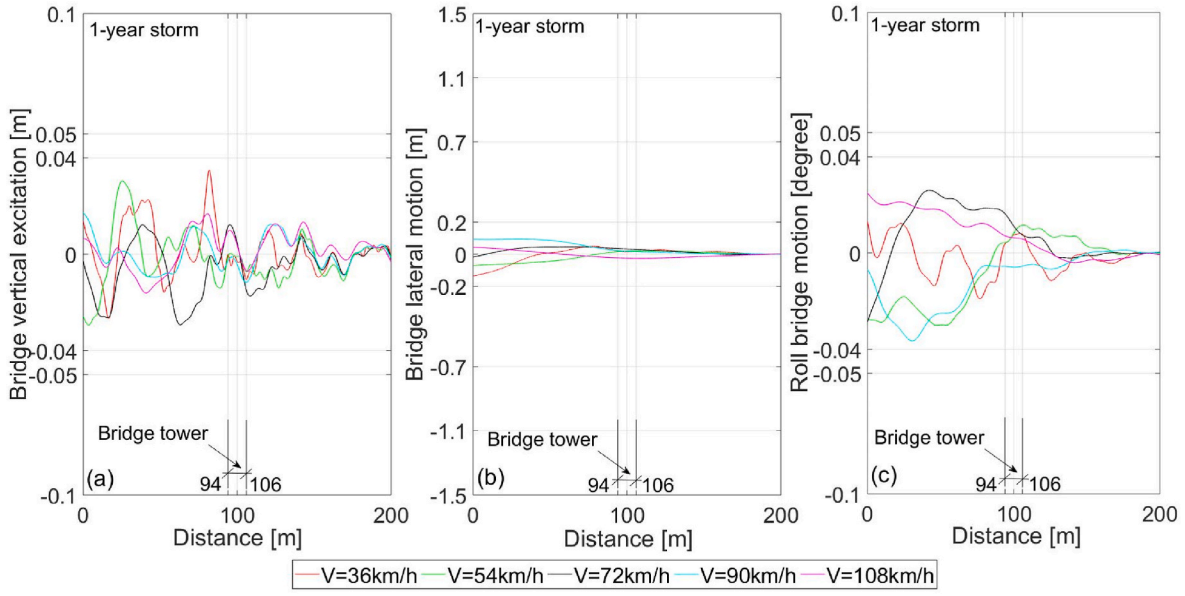

Fig. 12. Bridge deck excitations magnitudes around tower a) vertical; b) lateral and c) roll motions, as function of vehicle velocity for 1-year storm condition.

convention. A vehicle fixed coordinate system (ISO 8855) is attached to vehicle CoG.

Fig. 11 shows aerodynamic forces and moments as a function of distance for the one rigid body TS model, for the vehicle velocity of 36 km/h and the crosswind speed of 65 km/h. It could be noticed that side force value is close to zero (Fig. 11a), whereas wind rolling moment value changes its sign (Fig. 11b) when the vehicle is behind the tower. Changes in wind side force and yawing moment with a similar trend were confirmed in Refs. [2,4,5].

3. Vehicle models excitations

3.1. Bridge deck motions

On the south part, floating bridge deck is fixed with seabed by the tower (Fig. 1b). Bridge deck vertical, lateral and roll motions due to the wind and waves are insignificant near the tower. As an example, Fig. 12 presents vertical, lateral and roll bridge deck motions near to the bridge tower for the North-South direction under 1-year storm condition. Bridge vertical, lateral and roll motions are small values for every vehicle velocity, within ±0.04 m (Fig. 12a), ±0.02 m (Fig. 12b) and ±0.04° (Fig. 12c), respectively. Similar floating bridge deck excitations magnitudes around tower are confirmed for conditions more severe than 1-year storm (e.g. 100-year storm) [23]. Therefore, no bridge motions inputs in the vehicle models had been considered in the simulations. Detailed procedure for obtaining bridge motion inputs could be found in Refs. [6,18].

3.2. Wind forces and moments

Fig. 13 shows velocities of the crosswind component defined in the earth coordinate system (Fig. 9b) around the bridge tower as a function of distance and vehicle speeds for 1-year storm and 100-year storm conditions. Absolute of mean values of the crosswind velocities are

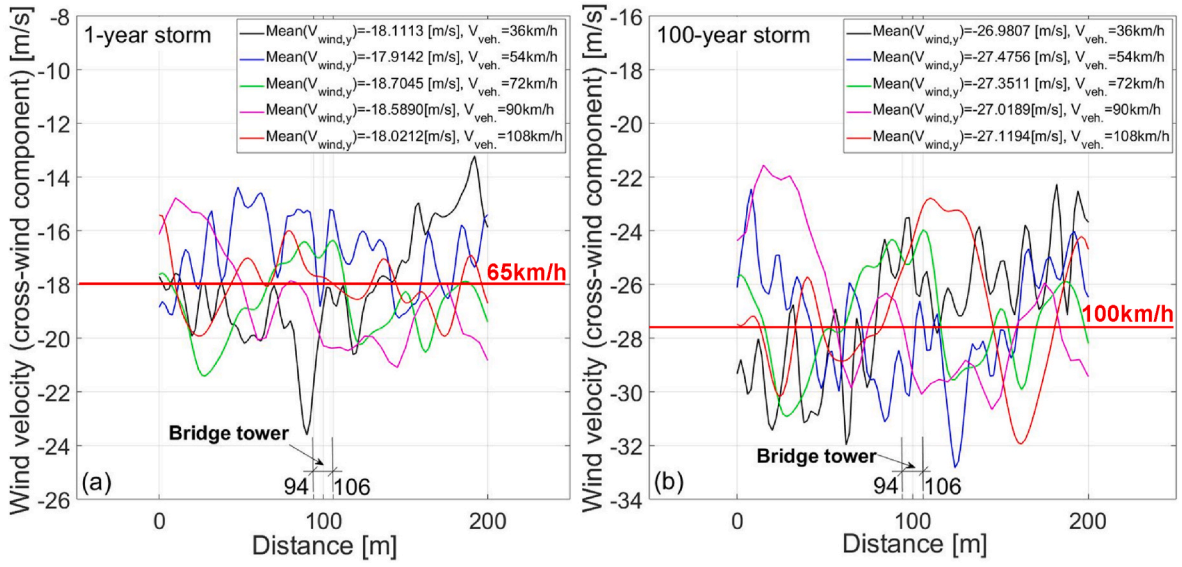

Fig. 13. Velocity of the cross-wind component around the floating bridge tower for a) 1-year storm; b) 100-year storm, as function of vehicle velocities.

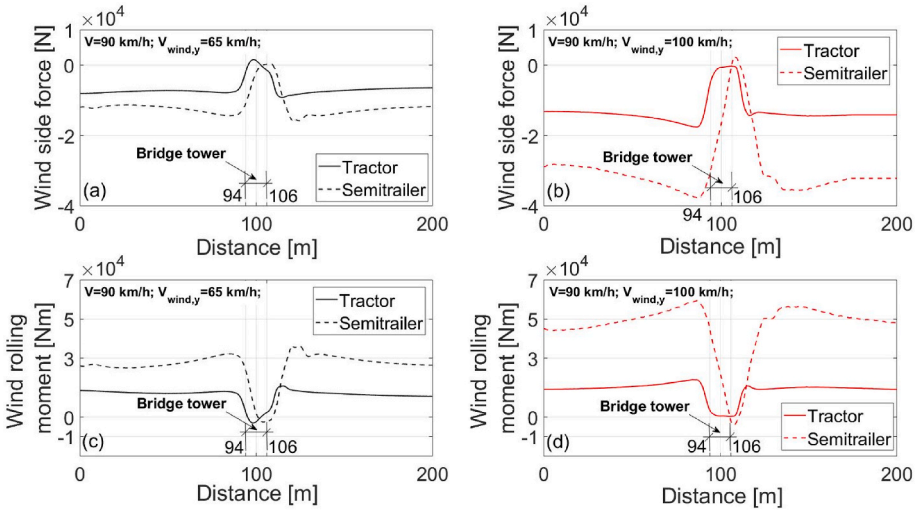

Fig. 14. Wind side force for the tractor and the semitrailer units for the crosswind speed of a) 65 km/h; b) 100 km/h and wind rolling moments for the tractor and the semitrailer units for the crosswind speed of c) 65 km/h; d) 100 km/h, for the vehicle velocity of 90 km/h.

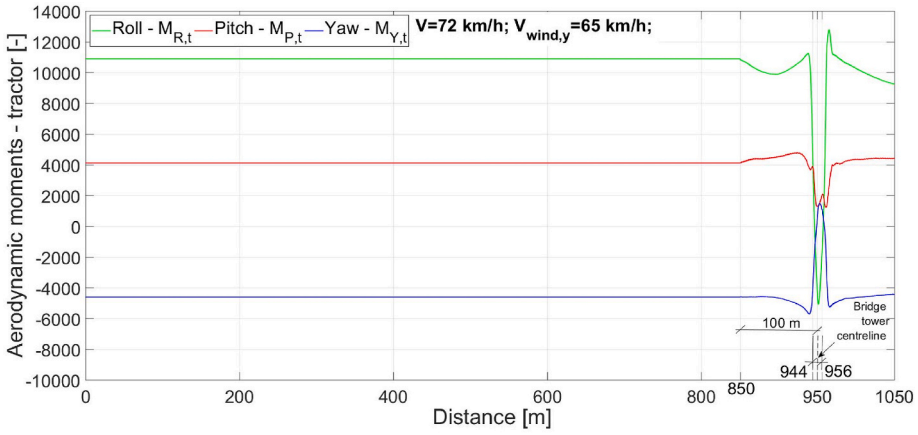

Fig. 15. Aerodynamic moments for the tractor unit as a function of distance for the vehicle velocity of 72 km/h and the crosswind speed of 65 km/h.

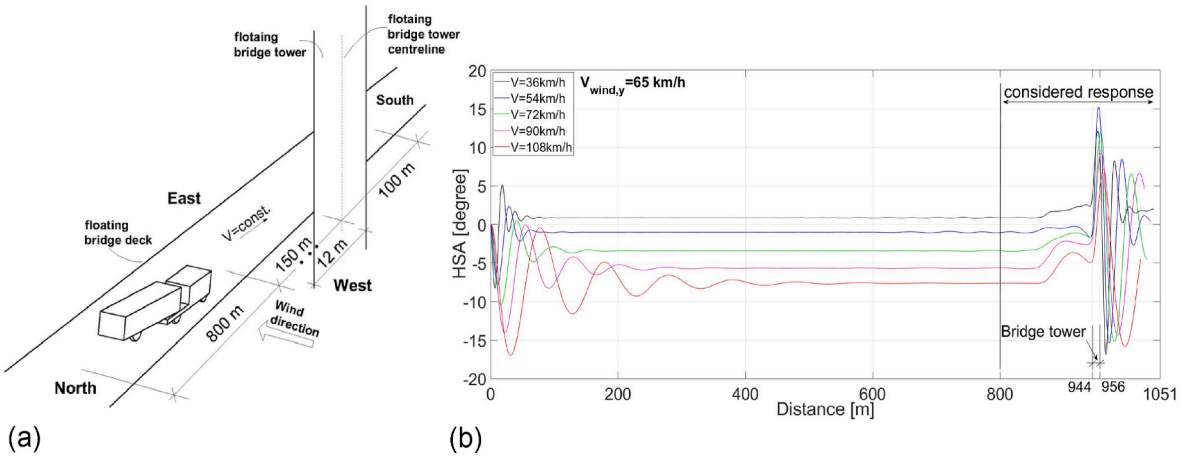

Fig. 16. TS a) on floating bridge deck with characteristic distances; b) HSA as a function of distance.

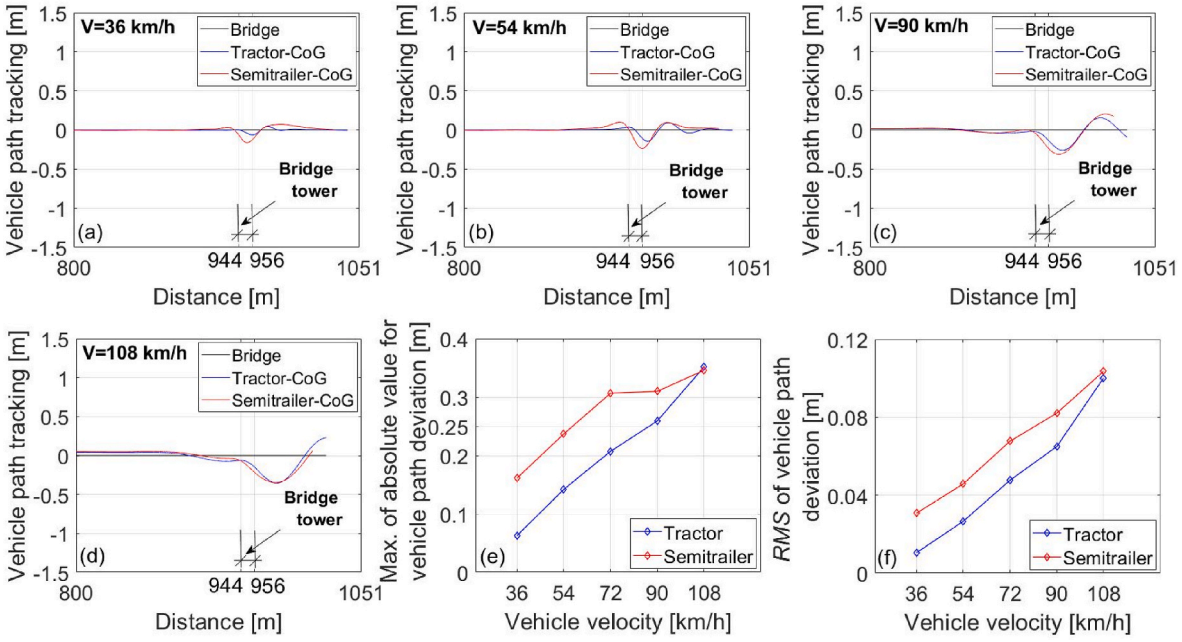

Fig. 17. Path tracking of TS units a) at 36 km/h; b) at 54 km/h; c) at 90 km/h; d) at 108 km/h; e) maximum of absolute value; f) RMS value for the crosswind speed of 65 km/h.

approximately 18 m/s (≈65 km/h) (Fig. 13a) and 27 m/s (≈100 km/h) (Fig. 13b) for 1-year storm and 100-year storm condition, respectively. Therefore, aerodynamic forces and moments acting on the vehicle had been calculated for the constant crosswind speeds of 65 km/h and 100 km/h in the CFD simulations.

As an example, Fig. 14a and b shows wind side forces for the tractor and the semitrailer units for the crosswind speeds of 65 km/h and 100 km/h and vehicle velocity of 90 km/h. For both vehicle units, wind side forces are higher values for the crosswind speed of 100 km/h. For the crosswind speed of 65 km/h, side forces for both units reach their max. negative values after the vehicle gets out of the tower (Fig. 14a). On the contrary, for the crosswind speed of 100 km/h, side forces for both units reach their max. negative values before the vehicle enters the tower (Fig. 14b). Side forces on both units decrease when vehicle is briefly shielded by the tower, and even change their signs. Characteristic changes in the side forces values might influence driver's ability to keep the vehicle on the intended path especially for the case of the strong crosswind.

Fig. 14c and d presents wind rolling moments for the vehicle units for the crosswind speeds of 65 km/h and 100 km/h and vehicle velocity of 90 km/h. Rolling moments on semitrailer unit decrease when vehicle is briefly shielded by the tower and change their signs. Changes in the rolling moments values might influence considerable vertical tyre forces shifts for the semitrailer and apparently rollover risk. Wind side forces and rolling moments have been used as the vehicle model excitation inputs when passing by the bridge tower in the simulation process.

3.3. *Driver's handwheel steering input*

In this paper, the driver model based on pure pursuit method defined earlier in Ref. [18] was used in the simulations. Driving simulator (CASTER) had been used for pure pursuit controller tuning, such as look-ahead time (LAT) value [18]. Detail description of the driver's model and its tuning for the heavy vehicle could be found in previous work [6,18]. Handwheel steer angle signals are used for assessing driver's effort in steering the vehicle when passing by the floating bridge tower (section 4.2).

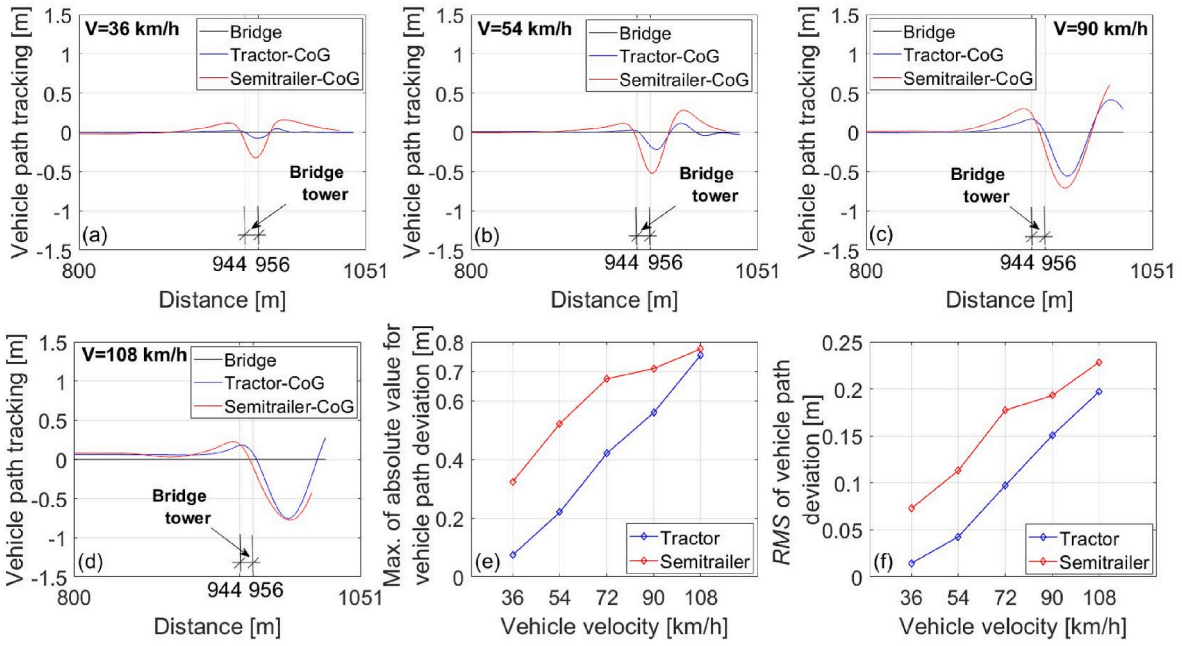

Fig. 18. Path tracking of TS units a) at 36 km/h; b) at 54 km/h; c) at 90 km/h; d) at 108 km/h; e) maximum of absolute value; f) RMS value for crosswind speed of 100 km/h.

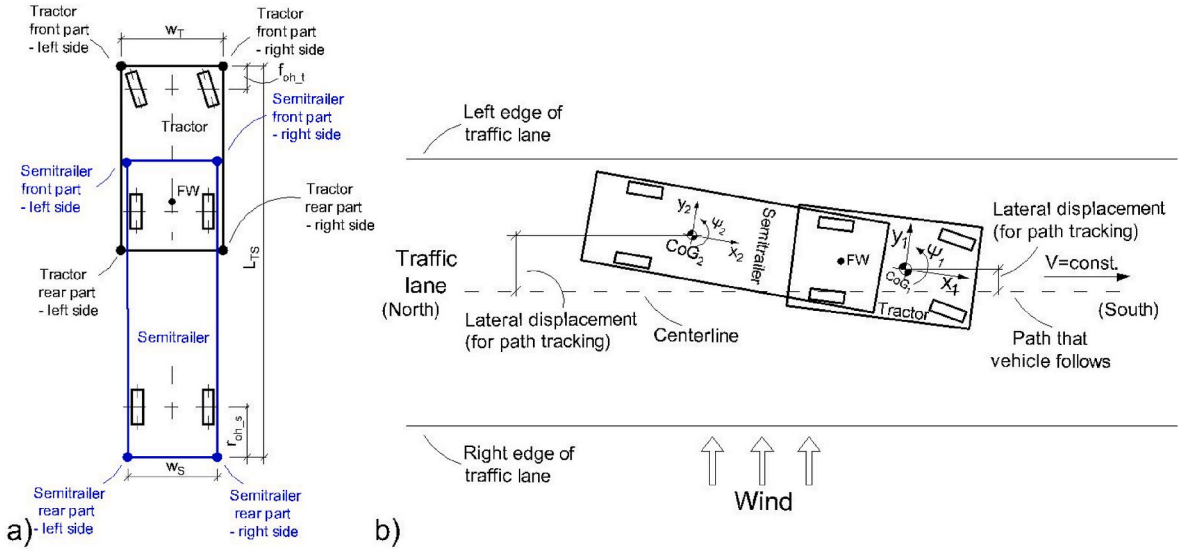

Fig. 19. TS a) outermost body points; b) position within the traffic lane and lateral displacement for path tracking.

4. Results of the simulation and discussion

For vehicle to achieve steady state motion, distance of 0.95 km before the bridge tower was considered as starting point for the vehicle movement (Fig. 16a). Constant values of aerodynamic forces and moments were used for the vehicle models excitations from starting point up to 100 m before the bridge tower centreline (Fig. 15). As an example, Fig. 15 presents aerodynamic rolling, pitching and yawing moments for the tractor unit as a function of distance for the vehicle velocity of 72 km/h and the crosswind speed of 65 km/h.

As an example, Fig. 16b shows the handwheel steer angle (HSA) for different vehicle velocity and the crosswind speed of 65 km/h as a function of travelled distance. Transient solution could be noticed at the beginning of the simulation for every vehicle velocity. Steady state solution appears after some distance travelled. It could be noticed that travelled distance for steady state increases with higher vehicle velocity. For example, for the vehicle velocity of 108 km/h steady state solution appeared after 600 m. In the analysis of the TS safe speeds all vehicle-driver responses have been considered after 800 m of travelled distance as denoted in Fig. 16b.

In the following section, proposed measures for safe vehicle speeds on Bjørnafjorden floating bridge will be presented. Measures have been defined in Refs. [6,18].

4.1. Lateral path deviation and risk of leaving the traffic lane

4.1.1. Vehicle path tracking

The aim of this section is to reveal how path tracking changes as function of a vehicle velocity. The lateral distance between the vehicle's CoG and the centreline of the traffic lane has been defined as the

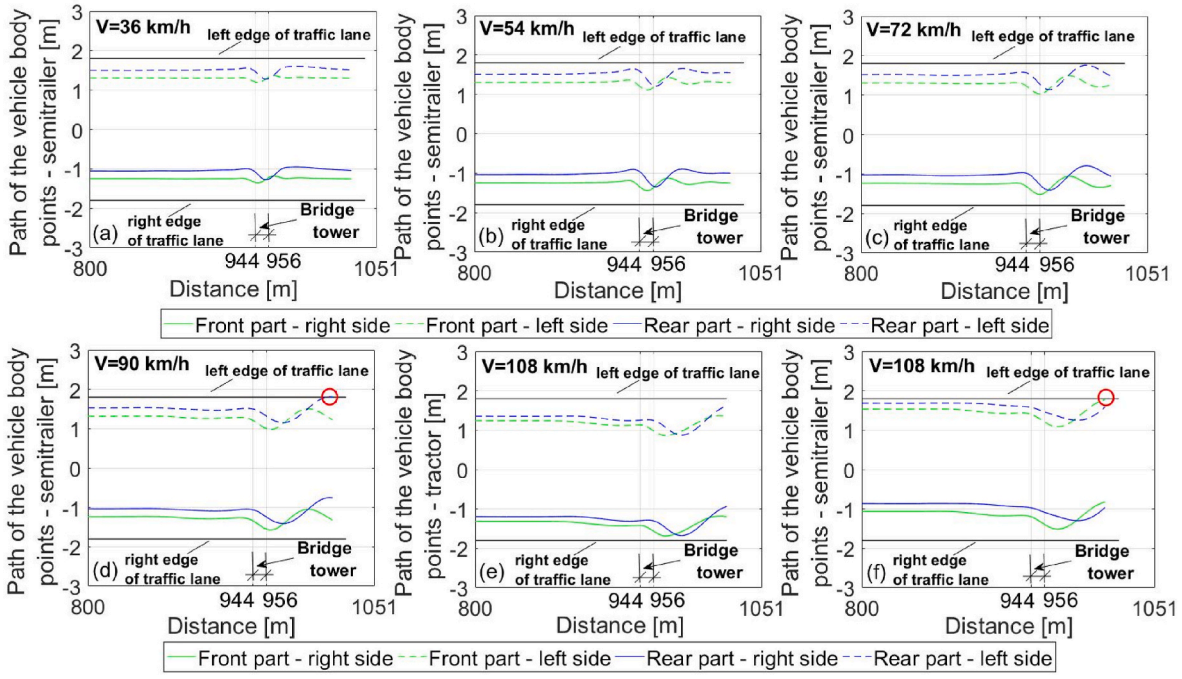

Fig. 20. Outermost body points for a) the semitrailer at speed 36 km/h; b) the semitrailer at speed 54 km/h; c) the semitrailer at speed 72 km/h; d) the semitrailer at speed 90 km/h; e) the tractor at speed 108 km/h; f) the semitrailer at speed 108 km/h, for the crosswind speed of 65 km/h.

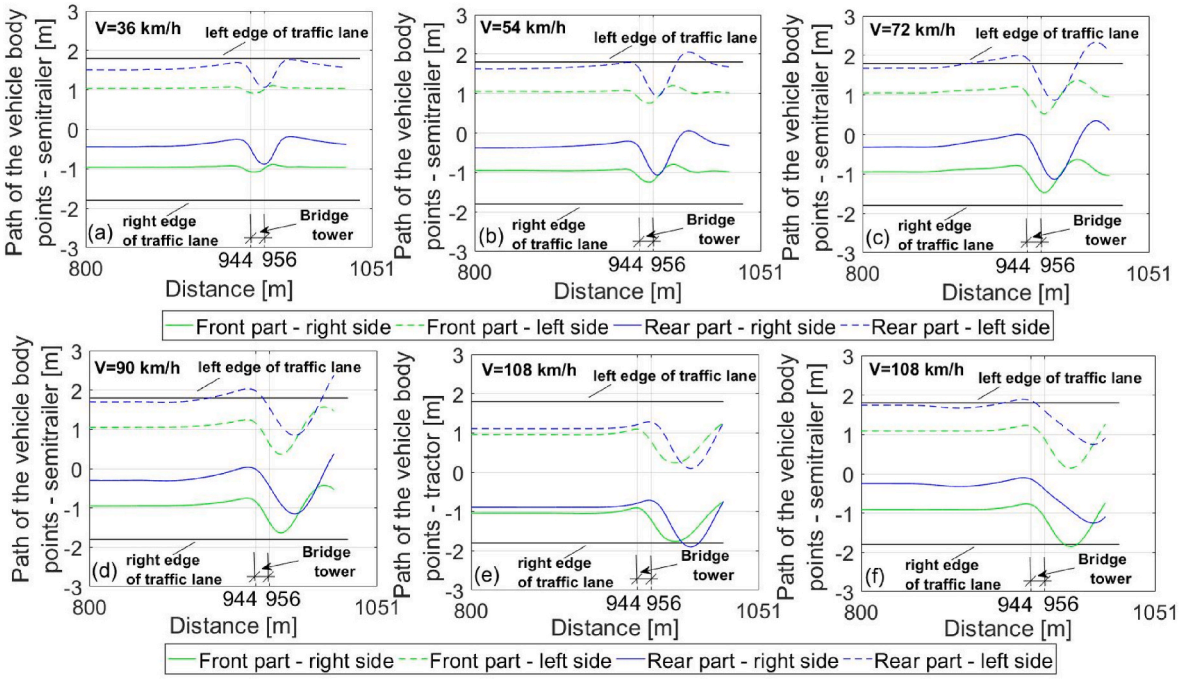

Fig. 21. Outermost body points for a) the semitrailer at speed 36 km/h; b) the semitrailer at speed 54 km/h; c) the semitrailer at speed 72 km/h; d) the semitrailer at speed 90 km/h; e) the tractor at speed 108 km/h; f) the semitrailer at speed 108 km/h, for the crosswind speed of 100 km/h.

measure for the path tracking (Fig. 19b). Simulation results for TS path tracking around the bridge tower under the crosswind speeds of 65 km/h and 100 km/h are presented in this section.

Fig. 17a–d presents path tracking for vehicle velocities of 36 km/h, 54 km/h, 90 km/h and 108 km/h for the crosswind speed of 65 km/h. Path deviation increases with the vehicle speed for both units (Fig. 17e and f). For the vehicle velocity of 90 km/h, path deviation for the tractor and the semitrailer units are 0.25 m and 0.3 m, respectively (Fig. 17e). Maximal path deviation of the semitrailer unit is higher in comparison with the tractor unit for velocities below 108 km/h (Fig. 17e). *RMS* value of the path deviation is higher for the semitrailer unit (Fig. 17f).

Fig. 18a–d presents path tracking for the vehicle velocities of 36 km/h, 54 km/h, 90 km/h and 108 km/h under the crosswind speed of 100 km/h. Path deviations are of high values for the high vehicle speeds. For the vehicle velocity of 90 km/h, path deviation for the tractor and the semitrailer units are close to 0.6 m and 0.7 m, respectively (Fig. 18e). For the vehicle velocity of 108 km/h, path deviation for both units is close to 0.8 m (Fig. 18e). The path deviations for both units are significantly

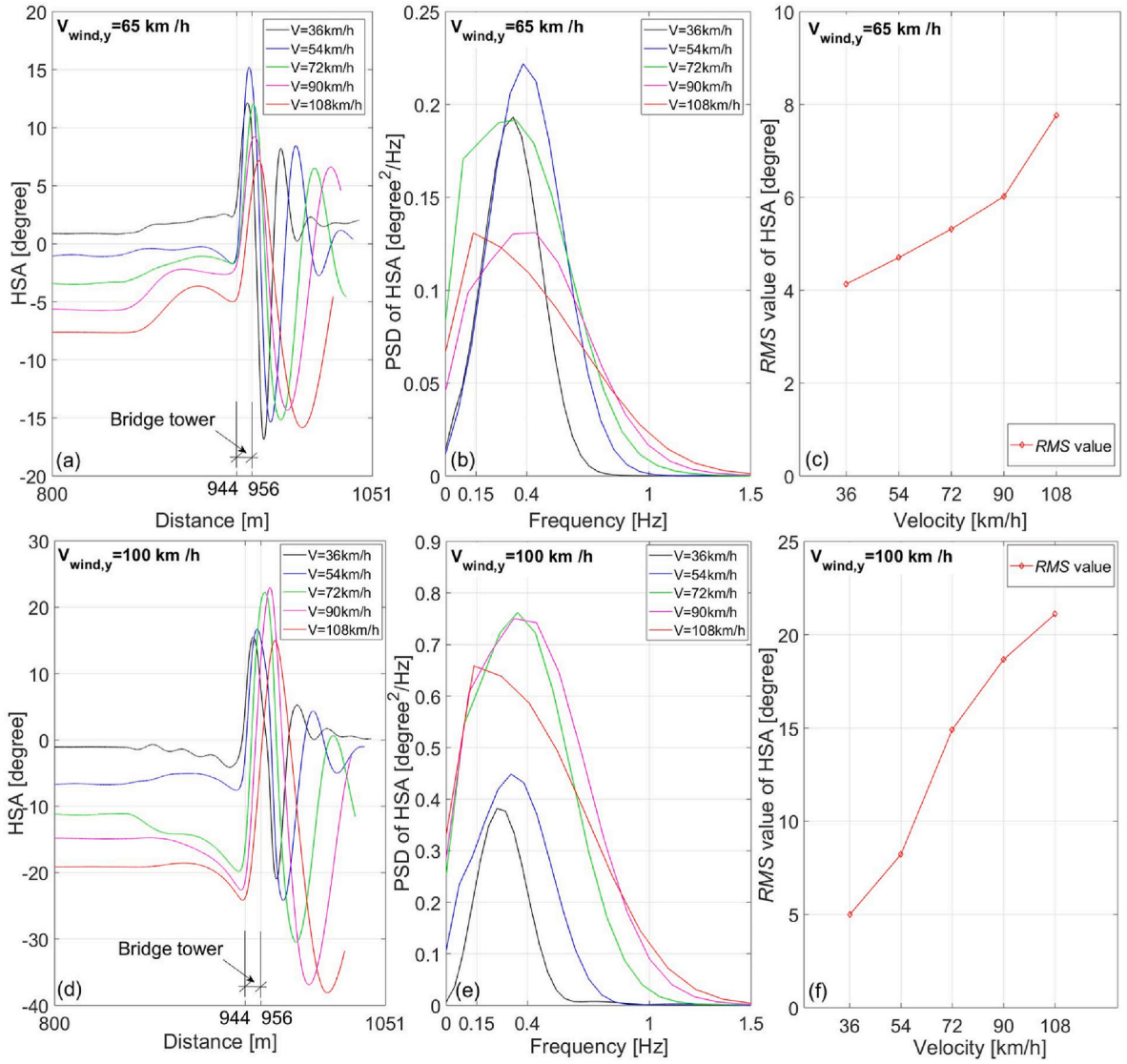

Fig. 22. HSA as a function of a) distance; b) frequency; c) RMS value, for different vehicle speeds and for crosswind speed of 65 km/h; and HSA as a function of d) distance; e) frequency; f) RMS value, for different vehicle speeds and for the crosswind speed of 100 km/h.

larger than those for the crosswind speed of 65 km/h (Fig. 18e; Fig. 17e).

4.1.2. *Traffic lane departure*

When passing by the bridge tower, path deviation of both vehicle units increases with the speed. It is of importance to reveal if TS leaves the traffic lane. Outermost vehicle body points are shown in Fig. 19a, whereas their position within the traffic lane in Fig. 19b.

Fig. 20 presents the outermost body points position within the traffic lane for the tractor and the semitrailer units for different vehicle velocities and the crosswind speed of 65 km/h. Simulation results show that the tractor unit stays within the traffic lane for every vehicle velocity. As an example, positions of the outermost tractor body points for the velocity of 108 km/h are shown in Fig. 20e. The outermost point at the rear-left side and front-left side of the semitrailer unit slightly leaves the traffic lane at 90 km/h and at 108 km/h soon after passing the bridge tower, denoted with red circles in Fig. 20d and f. Semitrailer unit stays in the traffic lane at and below velocity of 72 km/h.

Fig. 21 presents outermost body points position within the traffic lane for the tractor and the semitrailer units for different vehicle velocities and the crosswind speed of 100 km/h. At 54 km/h, 72 km/h, 90 km/h and 108 km/h the outermost point at the semitrailer rear-left side leaves the lane (Fig. 21b–f). The outermost point at the rear-right side of the tractor unit leaves the traffic lane at velocity of 108 km/h (Fig. 21e). Semitrailer unit does not leave the traffic lane at 36 km/h (Fig. 21a).

4.2. *Driver's effort when steering the vehicle around floating bridge tower*

The aim of this subsection is to investigate driver's effort in steering the vehicle when passing by the floating bridge tower under the influence of the crosswind. *RMS* value of HSA is appropriate measure for assessing driver's effort [18].

Fig. 22a presents the HSA as a function of travelled distance under the crosswind speed of 65 km/h. Absolute steady state HSA value increases with increasing vehicle velocity. HSA value of one degree compensates for the crosswind load at the vehicle speed of 36 km/h (Fig. 22a). For the vehicle speed of 108 km/h, steady state HSA value is −7° (Fig. 22a). HSA changes considerably when vehicle passing by the bridge tower to compensate for the lateral path deviation. It could be notice that the driver takes quick action to resist the wind shielding effects of the tower by steering the vehicle at a high angle. For example, for the vehicle speed of 54 km/h, HSA value is +15° (Fig. 22a). Another driver's quick action happens when the vehicle leaves the tower to compensate for excessive lateral displacement since of suddenly high side wind force. For instance, for the vehicle speed of 54 km/h, HSA

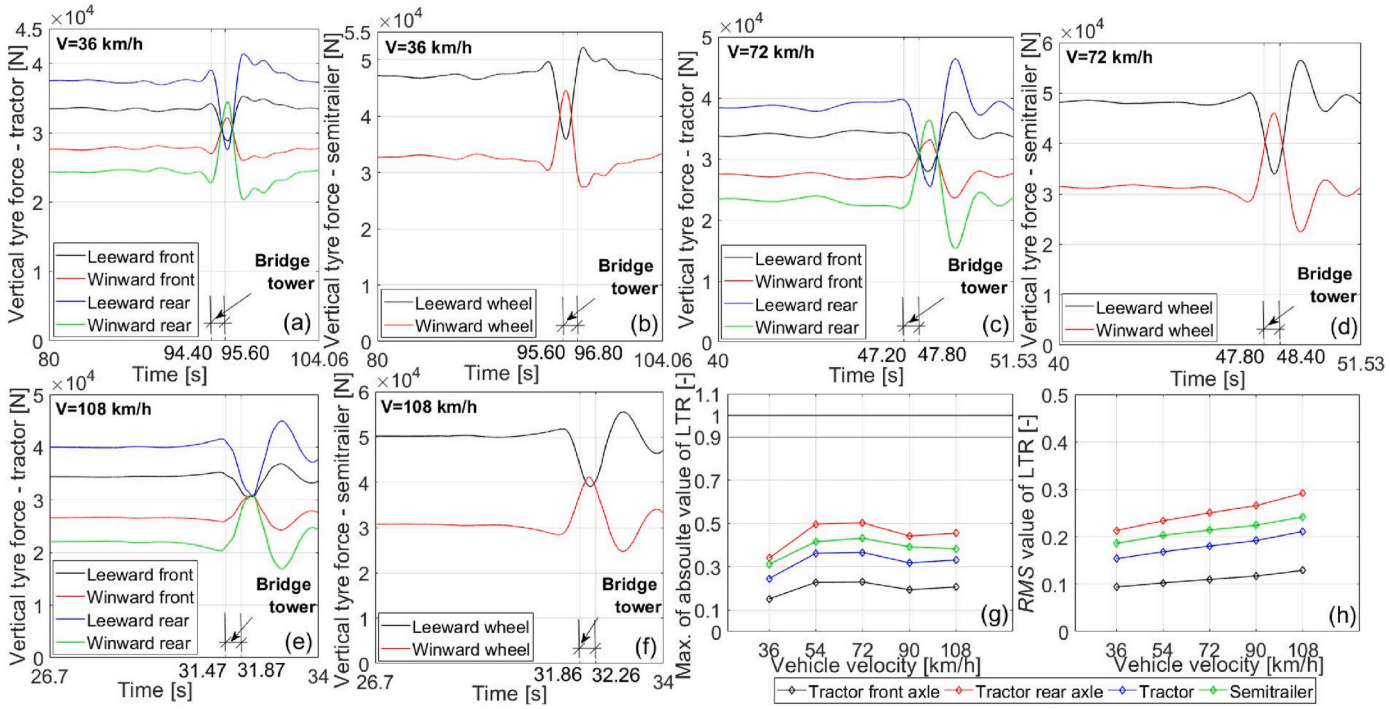

Fig. 23. VTFs for a) the tractor at 36 km/h; b) the semitrailer at 36 km/h; c) the tractor at 72 km/h; d) the semitrailer at 72 km/h; e) the tractor at 108 km/h; e) the semitrailer at 108 km/h, and g) maximum absolute LTR value; h) RMS value of LTR, for the crosswind speed of 65 km/h.

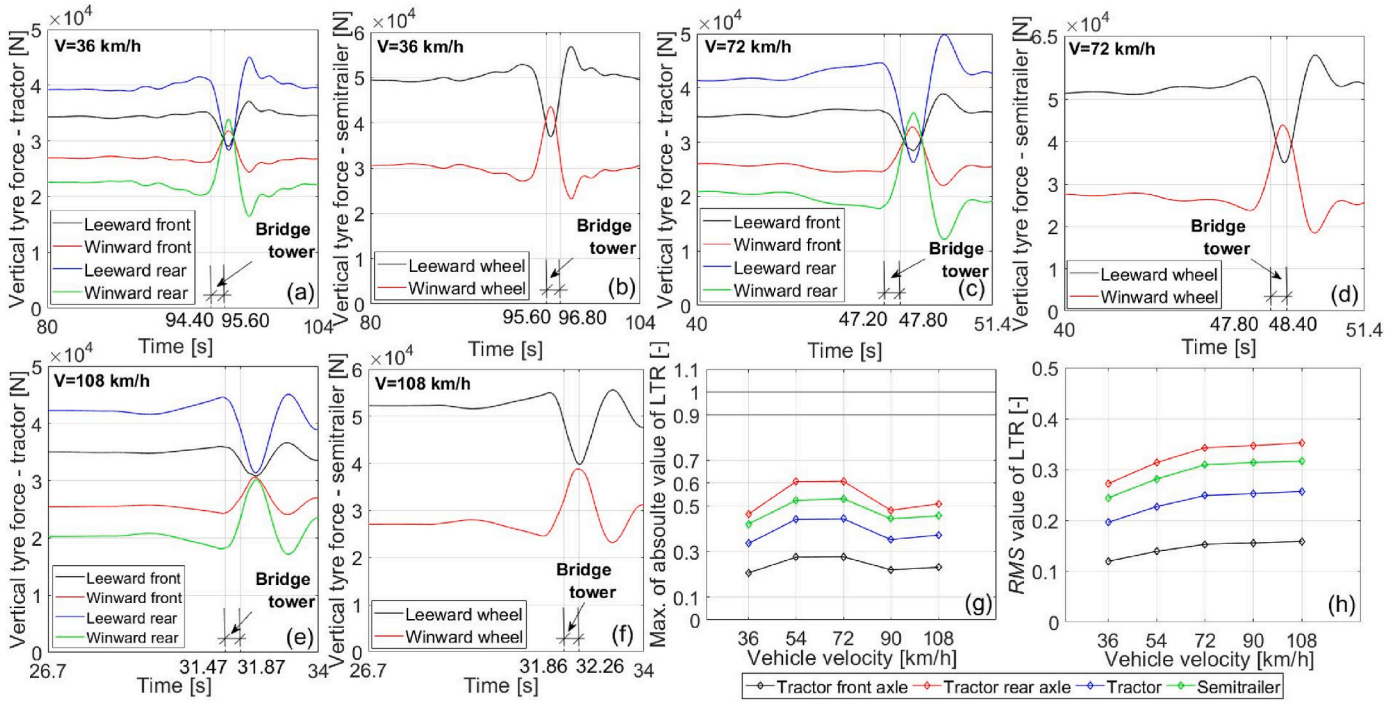

Fig. 24. VTFs for a) the tractor at 36 km/h; b) the semitrailer at 36 km/h; c) the tractor at 72 km/h; d) the semitrailer at 72 km/h; e) the tractor at 108 km/h; e) the semitrailer at 108 km/h, and g) maximum absolute LTR value; h) RMS value of LTR, for the crosswind speed of 100 km/h.

value is a little over −15° (Fig. 22a).

Fig. 22b shows PSD of HSA for different vehicle speeds. The HSA's intensities are less than 1.5 Hz. The highest intensity for the lower vehicle speeds of 36 km/h and 54 km/h are at the around 0.4 Hz, whereas for the high speed of 108 km/h around 0.15 Hz. Fig. 22c presents *RMS* value of HSA. *RMS* value increases with the vehicle velocity. *RMS* value is +8° at 108 km/h (Fig. 22c).

Fig. 22d presents HSA in function of distance under the crosswind speed of 100 km/h. Absolute steady state values of HSA are higher compared to those for the crosswind speed of 65 km/h. For the vehicle speed of 108 km/h, steady state HSA value is around −20° (Fig. 22d). For the vehicle speed of 90 km/h, maximum value of HSA is around +20° whereas minimum value is −37° (Fig. 22d). The highest HSA intensities are concentrated around 0.4 Hz for the vehicle speeds of 72 km/

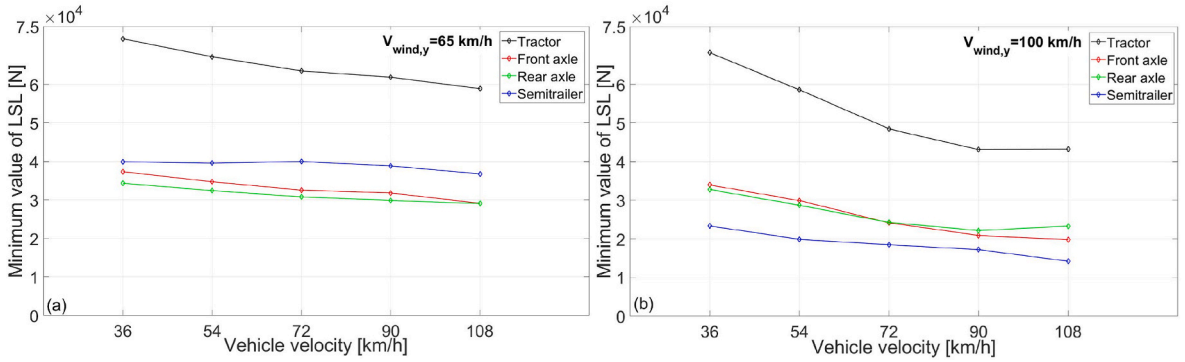

Fig. 25. Minimum value of the LSL parameter as a function of vehicle velocity for a) the crosswind speed of 65 km/h; b) the crosswind speed of 100 km/h.

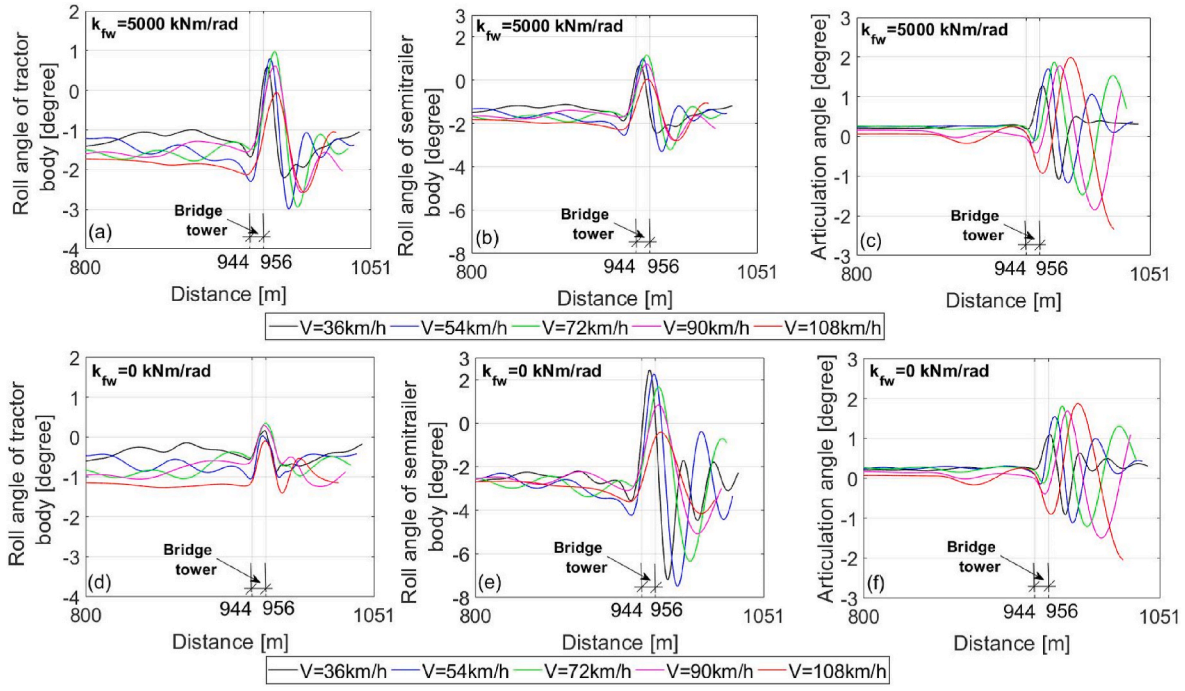

Fig. 26. TS model responses for the crosswind speed of 65 km/h a) roll angle of the tractor body; b) roll angle of the semitrailer body; c) articulation angle, for the roll-stiffness of k_{fw} = 5000 kNm/rad; d) roll angle of the tractor body; e) roll angle of the semitrailer body and f) articulation angle, for the roll-stiffness of k_{fw} = 0 kNm/rad.

h, 90 km/h and 108 km/h (Fig. 22e). *RMS* values are higher than those for the crosswind speed of 65 km/h (Fig. 22c). *RMS* value is around 20° at 108 km/h (Fig. 22f).

4.3. Risk of vehicle roll-over

Passing by the tower under the crosswind might cause vehicle-driver responses leading to hazardous situation such as a vehicle roll-over. The aim of this subsection is to investigate risk of vehicle roll-over considering load transfer ratio (LTR) values [18].

Fig. 23a–f presents vertical tyre forces (VTFs) for the tractor and the semitrailer units as a function of time and velocities for the crosswind speed of 65 km/h. It could be seen that vertical force on the tractor windward rear wheel decreases with velocity, but the values are above zero. Similarly, vertical force on the semitrailer windward wheel decreases with velocity and stays above zero. No risk of TS rollover is confirmed with the LTR values (Fig. 22g). Tractor rear axle has the highest LTR values of 0.5 at velocities of 54 km/h and 72 km/h (Fig. 22g). *RMS* values of LTR increase with the vehicle velocity for each axle and both units (Fig. 22h).

Fig. 24a–f shows VTFs for the tractor and the semitrailer units as a function of time and velocities for the crosswind speed of 100 km/h. Vertical forces on the windward wheels for both units decrease with velocity and are greater than zero. Tractor rear axle has the highest LTR values of 0.6 at velocities of 54 km/h and 72 km/h (Fig. 24g).

4.3.1. Assessment of TS sideslip

Intensive lateral tyre forces due to driver's response might exceed maximum allowable lateral friction forces. The aim of this subsection is to investigate risk of TS sideslip by Lateral Sideslip Limit (LSL) parameter [18].

The risk of TS sideslip could be investigated considering LSL parameter for the vehicle axles and for the whole vehicle [24,25]. LSL parameter for the vehicle axle is given by Eq. (13)

$$LSL_i = \min\left[F_{y,i}^{max} - F_{y,i}\right] = \min\left[\mu \cdot Z_{t,i} - F_{y,i}\right] \geqslant 0 \tag{13}$$

where i=*fa,ra,sa* refer to front, rear and semitrailer axle; $F_{y,i}^{max}$ are the maximum values of the lateral tyre forces that could be achieved on the axle, for a particular surface of the road; $Z_{t,i}$ are the normal tyre forces on

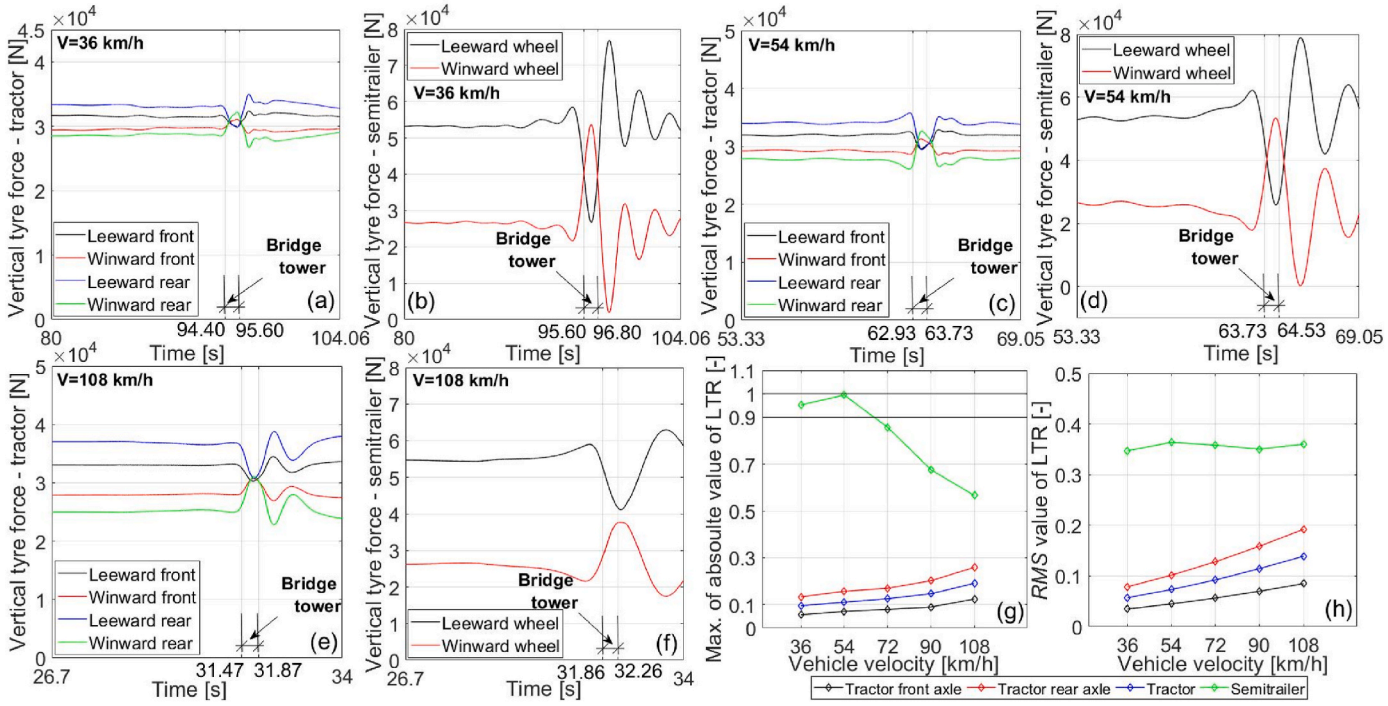

Fig. 27. VTFs for TS model with no roll-stiffness in FW under the crosswind speed of 65 km/h a) the tractor at 36 km/h; b) the semitrailer at 36 km/h; c) the tractor at 54 km/h; d) the semitrailer at 54 km/h; e) the tractor at 108 km/h; f) the semitrailer at 108 km/h, and g) maximum absolute LTR value; h) RMS value of LTR.

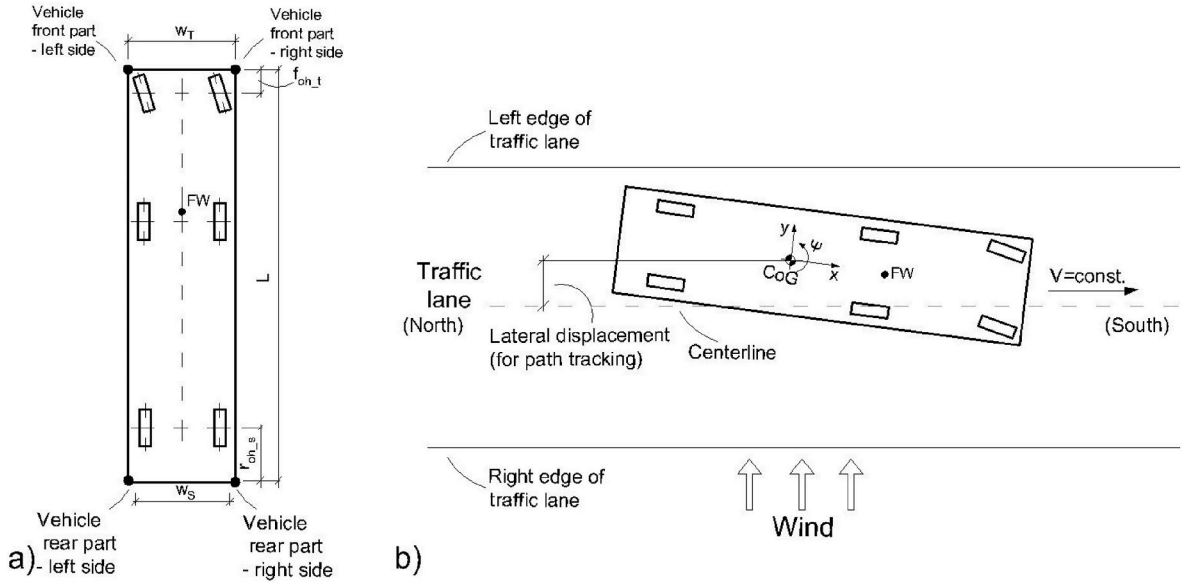

Fig. 28. One rigid body TS model a) the outermost body points; b) position within the traffic lane.

the axle; $F_{y,i}$ are the lateral tire forces for vehicle axle; and μ is coefficient of the road friction. TS sideslips when the LSL value is lower than zero.

Minimum values of the LSL parameter for the tractor axle and both units as function of vehicle velocity for the crosswind speeds of 65 km/h and 100 km/h is shown in Fig. 25. LSL values decrease with vehicle velocity for both crosswind speeds. The tractor rear axle has the lowest LSL values for the crosswind speed of 65 km/h (Fig. 25a) whereas the semitrailer axle for the crosswind speed of 100 km/h (Fig. 25b). TS does not sideslip since LSL values are higher than zero for dry/wet road surface (road friction coefficient of 0.7 peak value).

4.4. Comparison between different ways to model the TS

This section presents TS models responses considering different ways of coupling in the FW. The differences between TS models responses (e.g. maximum absolute LTR value, position of outermost body points) explains the importance of appropriate mathematical modelling of TS vehicle.

4.4.1. Responses of TS model coupled in roll

The main aim of this subsection is to investigate roll-over risk for TS model which is roll moment free in the FW considering vertical tyre forces and LTR values.

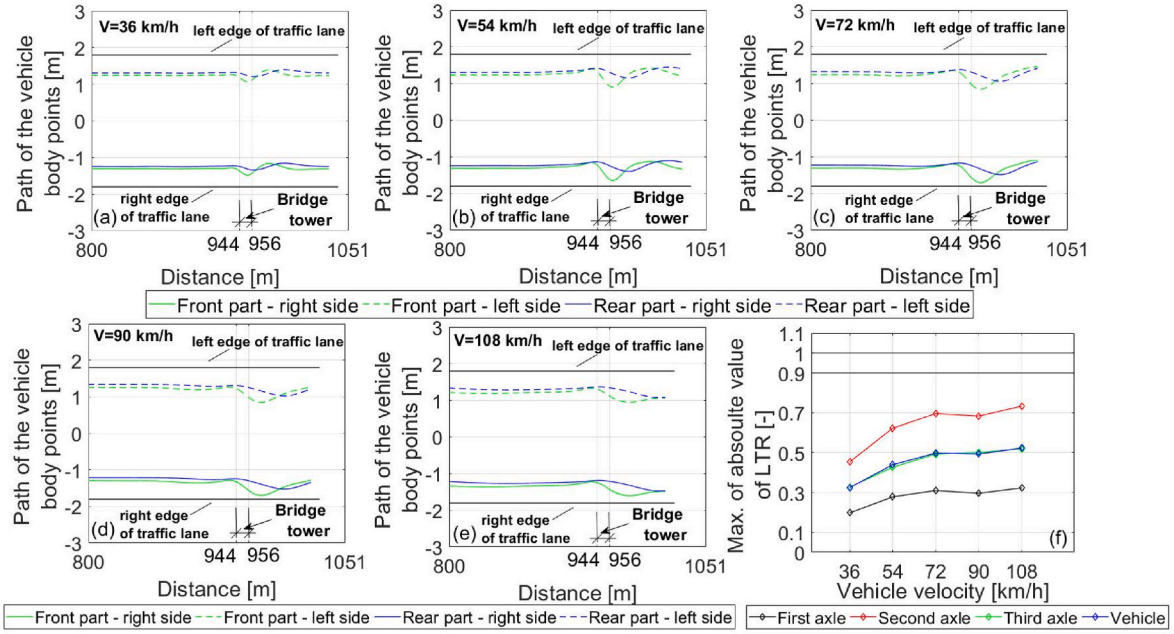

Fig. 29. One rigid body TS model outermost body point at speed of a) 36 km/h; b) 54 km/h; c) 72 km/h; d) 90 km/h; e) 108 km/h; and f) maximum absolute LTR value, for the crosswind speed of 65 km/h.

Fig. 26 presents TS model responses (roll and articulation angles) for the crosswind speed of 65 km/h. Body roll angles for both units are similar values for the TS model with the roll-stiffness of k_{fw}=5000 kN/rad in the FW (Fig. 26a and b). For instance, steady state roll angle value for both units is close to $-2°$ for the vehicle velocity of 108 km/h. Further, two peak values occur due to the driver's HSA input when the vehicle passing by the tower. For example, the first peak value of $+1°$ and the second peak value of around $-3°$ at velocities of 54 km/h and 72 km/h (Fig. 26a and b). When roll-stiffness is not considered (k_{fw}=0 kN/rad), two TS units roll independently. It could be noticed that roll angles for the tractor unit are lower values than those for the semitrailer unit (Fig. 26d and e). Also, the tractor body roll angles are smaller values compared to those from TS model coupled in roll (Fig. 26a and d). It is opposite for the semitrailer unit (Fig. 26b and e).

Roll-stiffness does not have significant influence on the differences in the articulation angle values (Fig. 26c and f). For example, for both TS models articulation angle amplitudes are $\pm 2°$ at 108 km/h (Fig. 26c–f).

Fig. 27 presents VTFs for the TS model without roll-stiffness in FW for the crosswind speed of 65 km/h. Load transfer from the tractor windward to leeward wheels is less pronounced especially at lower vehicle velocities (Fig. 27a) in comparison with TS model with roll-stiffness (Fig. 24a). For the semitrailer unit, load transfer from the windward to leeward wheel is more pronounced at the lower vehicle velocities (at 36 km/h and 54 km/h). At these speeds VTFs on the semitrailer windward wheel is close to zero indicating roll over risk for this unit (Fig. 27b and d). LTR values are higher than 0.9 at the vehicle velocities of 36 km/h and 54 km/h (Fig. 27g). These characteristic changes in the VTFs could be explained considering the roll eigenfrequency of the vehicle in combination with the passing time behind the tower.

4.4.2. *Responses of TS model rigidly coupled in roll and yaw*

The aim of this subsection is to investigate position of the outermost points within the traffic lane for TS model rigidly coupled in the FW. Fig. 28a shows the outermost points of one rigid body TS model. Fig. 28b shows their position within the traffic lane.

Fig. 29a–e presents outermost body points position within the traffic lane for one rigid body TS model for different vehicle velocities and the crosswind speed of 65 km/h. Vehicle stays in the traffic lane for every velocity unlike TS model with articulation angle considered (Fig. 20).

Fig. 29f shows maximum of absolute LTR value. Vehicle second axle has the highest LTR value, but these values are below 0.9. For example, LTR value is close to 0.7 for vehicle speed of 108 km/h (Fig. 29f). LTR value for the whole vehicle is increasing with the vehicle speed (Fig. 29f). The same conclusion has been confirmed in Ref. [2]. LTR value for the whole vehicle is lower than 0.9 (Fig. 29f), and the same has been confirmed in Ref. [2].

5. Conclusions

As stated main objective, safe velocities for a heavy articulated vehicle when passing by Bjørnafjorden floating bridge tower under the influence of different constant crosswind speeds (65 km/h and 100 km/h) were recommended. The recommendation is based on the TS model with FW coupling in roll and free in yaw. Furthermore, important responses from TS models that are roll moment free and rigidly coupled have been analysed to investigate the influence of different ways of FW modelling on safe speed assessments. Analysis reveals importance of appropriate mathematical modelling of an articulated vehicle when passing bridge tower.

The main conclusions from this research are as follows:

- Path deviation of the tractor and the semitrailer units increase with vehicle speed and with the crosswind speeds. Path deviation for the semitrailer unit is larger than for the tractor unit for the vehicle velocities up to 90 km/h for both crosswind speeds.
- Tractor unit leaves the traffic lane at higher vehicle velocity and higher crosswind speed after passing the bridge tower. Semitrailer unit leaves the traffic lane at lower vehicle velocity and higher crosswind speed after passing the bridge tower.
- Tractor rear axle has the highest LTR values at velocities of 54 km/h and 72 km/h for both crosswind speeds. Those LTR values are below threshold of 0.9 meaning that no rollover risk happens when TS passing by the tower.
- Absolute steady state HSA value increases with vehicle velocity for both crosswind speeds. Absolute steady state HSA are higher values for the crosswind speed of 100 km/h than for the crosswind speed of 65 km/h.

- HSA changes considerably when the vehicle passing by the bridge tower to compensate for lateral path deviation. Firstly, high HSA value appears to resist the wind shielding effects of the tower. Secondly, high HSA value appears when the vehicle leaves the tower to compensate for excessive lateral displacement since of sudden side wind force.
- LSL values are greater than zero for every vehicle velocity meaning that there is no risk of TS sideslip for dry/wet road surface (road friction coefficient of 0.7 peak value).
- TS safe velocity decreases with the crosswind speed. TS can safely pass by the tower at and below velocity of 72 km/h and at velocity of 36 km/h for the crosswind speeds of 65 km/h and 100 km/h, respectively.
- Roll-stiffness in the FW has a significant influence on load transfer from windward to leeward wheels, and apparently assessment of TS safe speed. For TS model free in roll, roll-over risk is noticeable at lower vehicle velocities (at 36 km/h and 54 km/h). At these velocities LTR values are higher than threshold of 0.9.
- Unlike TS model coupled in roll, TS model rigidly coupled stays in the traffic lane for every considered vehicle velocity under the crosswind speed of 65 km/h. Rigid connection in the FW underestimates TS safe speed assessments when vehicle passing by the bridge tower.

The Bjørnafjorden floating bridge is part of the E39 coastal highway route road project in Norway and is currently in its design phase. Therefore, experimental investigation of the vehicle's behaviour when passing bridge tower and verification of the validity of the vehicle models are planned for future work.

CRediT authorship contribution statement

Dragan Sekulic: Writing – original draft, Visualization, Methodology, Investigation, Data curation, Conceptualization. **Alexey Vdovin:** Supervision, Conceptualization. **Bengt Jacobson:** Validation, Supervision, Methodology, Conceptualization. **Simone Sebben:** Supervision, Conceptualization. **Stian Moe Johannesen:** Resources, Investigation.

Declaration of competing interest

The authors declare that they have no known competing financial interests or personal relationships that could have appeared to influence the work reported in this paper.

Data availability

Data will be made available on request.

Acknowledgements

The Norwegian Public Roads Administration (NPRA) provided support for this research. This support is gratefully acknowledged. The CFD computations were enabled by resources provided by the National Academic Infrastructure for Supercomputing in Sweden (NAISS) and the Swedish National Infrastructure for Computing (SNIC) at National Supercomputer Centre (NSC) and Chalmers' Centre for Computational Science and Engineering (C3SE) partially funded by the Swedish Research Council through grant agreements no. 2022–06725 and no. 2018–05973.

Appendix

Table 1
TS parameters (applied for 9 DOF and 7 DOF TS models).

Geometric parameters of the tractor unit and semitrailer unit	
Wheelbase of the tractor, L_t [m]	5.95
Distance from the tractor CoG to its front axle, l_{ft} [m]	3.00
Distance from the tractor CoG to its rear axle, l_{rt} [m]	2.95
Distance from the tractor front axle CoG to the front right/left wheel, b_f [m]	1.00
Distance from the tractor rear axle CoG to the rear right/left wheel, b_r [m]	1.00
Distance from the ground to the tractor CoG, $h_{CoG,t}$ [m]	1.16
Distance from the tractor FW to the tractor CoG, a [m]	2.75
Distance from the ground to the tractor roll-centre, h_{RCt} [m]	0.6306
Height of the tractor front axle roll-centre, $h_{RCfa.}$ [m]	0.6306
Height of the tractor rear axle roll-centre, $h_{RCra,}$ [m]	0.6306
Distance from the tractor CoG to the roll-centre of the front axle, Δh_{sf} [m]	0.5294
Distance from the CoG to the roll-centre of the rear axle, Δh_{sr} [m]	0.5294
Distance from suspension elements on the tractor front axle to the front axle CoG, e_{u1} [m]	0.70
Distance from suspension elements on the tractor rear axle to the rear axle CoG, e_{u2} [m]	0.80
Wheelbase of the semitrailer, L_s [m]	11.08
Distance from the semitrailer CoG to the fifth-wheel, l_{s1} [m]	9.18
Distance from the semitrailer CoG to its axis, l_{s2} [m]	1.19
Distance from the semitrailer right/left wheel to its axle CoG, b_s [m]	1.00
Height of the semitrailer CoG, $h_{CoG,s.}$ [m]	1.724
Distance from the ground to the semitrailer axle roll-centre, $h_{RCsa.}$ [m]	0.6306
Distance from the semitrailer CoG to the roll-centre for its axle, Δh_{ss} [m]	1.0934
Height of the semitrailer roll-centre, h_{RCs} [m]	1.0765
Distance from suspension elements on the semitrailer axle to its CoG, e_{us} [m]	0.80
Length of the tractor-semitrailer combination, L_{TS} [m]	20.51
Width of the tractor-semitrailer combination, W_T, W_S [m]	2.55
Front overhang, $f_{oh,t}$	1.50
Rear overhang, $r_{oh,s}$	2.80
Distance from the vehicle first axle to its second axle (the one rigid body model), l_1 [m]	5.95
Distance from the vehicle second axle to its CoG (the one rigid body model), l_2 [m]	2.74
Distance from the vehicle third axle to its CoG (the one rigid body model), l_3 [m]	8.09
Distance from the vehicle CoG to the ground (the one rigid body model), h_{CoG} [m]	1.4292
Height of the vehicle roll-centre (the one rigid body model), h_{RC} [m]	0.6306

(*continued on next page*)

Table 1 (*continued*)

Geometric parameters of the tractor unit and semitrailer unit	
Distance from the vehicle CoG to the roll-centres of the axles (the one rigid body model), $\Delta h_{s(f,r,s)}$ [m]	0.7986
Mass parameters of the tractorunit and semitrailer unit	
Sprung mass of the tractor, $m_{sm,t}$ [kg]	8739
Mass of the tractor front axle, m_{fa} [kg]	746
Mass of the tractor rear axle, m_{ra} [kg]	1355
Moment of inertia about its x-axis of the tractor sprung mass, $J_{t,x}$ [kgm^2]	15000
Moment of inertia about its x-axis of the tractor front axle, $J_{fa,x}$ [kgm^2]	315
Moment of inertia about its x-axis of the tractor rear axle, $J_{ra,x}$ [kgm^2]	657
Moment of inertia about its z-axis of the tractor, $J_{t,z}$ [kgm^2]	21500
Empty semitrailer sprung mass, $m_{sm,s}$ [kg]	8100
Equivalent semitrailer axle mass, m_{sa} [kg]	1800
Moment of inertia about its x-axis of semitrailer sprung mass, $J_{s,x}$ [kgm^2]	85500
Equivalent semitrailer axle moment of inertia relative to its x_{sa}-axis, $J_{sa,x}$ [kgm^2]	750
Semitrailer moment of inertia about its z-axis, $J_{s,z}$ [kgm^2]	151000
Vehicle sprung mass (the one rigid body model), m_{sm} [kg]	16839
Vehicle first axle mass (the one rigid body model), m_{fa} [kg]	746
Vehicle second axle mass (the one rigid body model), m_{sa} [kg]	1355
Vehicle third axle mass (the one rigid body model), m_{ta} [kg]	1800
Vehicle sprung mass moment of inertia about its x-axis (the one rigid body model), J_x [kgm^2]	100500
Vehicle sprung mass moment of inertia about its z-axis (the one rigid body model), J_z [kgm^2]	187370
Oscillatory parameters of the tractor unit and semitrailer unit	
Stiffness of the air spring - tractor front axle, k_{sfl}, k_{sfr} [N/m]	175000
Damping of the single shock-absorber - tractor front axle, $c_{d,fa}$ [Ns/m]	20000
Damping of the equivalent shock-absorber on the left/right side - tractor front axle, c_{dfl}, c_{dfr} [Ns/m]	40000
Stiffness of the single air spring - tractor rear axle, $k_{s,ra}$ [N/m]	200000
Stiffness of the equivalent air spring on the left/right side - tractor rear axle, k_{srl}, k_{srr} [N/m]	400000
Damping of the single shock-absorber - tractor rear axle, $c_{d,ra}$ [Ns/m]	22500
Damping of the equivalent shock-absorber on the left/right side - tractor rear axle, c_{drl}, c_{drr} [Ns/m]	45000
Stiffness of the single tire radial on the left/right side - tractor front axle, k_{tfl}, k_{tfr} [N/m]	1000000
Stiffness of the equivalent tire radial on the left/right side - tractor rear axle, k_{trl}, k_{trr} [N/m]	4000000
Stiffness of the single air spring - semitrailer axle, $k_{s,sa}$ [N/m]	200000
Stiffness of the equivalent air spring on the left/right side - semitrailer axle, k_{sr}, k_{sl} [N/m]	400000
Damping of the single shock-absorber - semitrailer axle, $c_{d,sa}$ [Ns/m]	22500
Damping of the equivalent shock-absorber on the left/right side - semitrailer axle, c_{dl}, c_{dr} [Ns/m]	45000
Stiffness of the single tire radial on the left/right side - semitrailer axle, k_{tfl}, k_{tfr} [N/m]	1000000
Stiffness of the equivalent tire radial on the left/right side - semitrailer axle, k_{tsl}, k_{tsr} [N/m]	6000000
Torsional stiffness of the anti-roll bar - tractor front axle, $k_{arb,fa}$ [Nm/rad]	120000
Torsional stiffness of the anti-roll bar - tractor rear axle, $k_{arb,ra}$ [Nm/rad]	120000
Torsional stiffness of the anti-roll bar - semitrailer axle, $k_{arb,sa}$ [Nm/rad]	120000
Spring of the rotational stiffness in FW (modified TS model), k_{fw} [Nm/rad]	500000

Table 2
Abbreviations, notations and other parameters.

Abbreviations
Tractor-semitrailer (TS)
Fifth-wheel (FW)
Computational Fluid Dynamics (CFD)
Degrees of Freedom (DOF)
Centre of Gravity (CoG)
Notations
Vehicle fixed coordinate systems - ISO 8855
Reference coordinate systems for CFD simulations - ISO 4130
Other parameters
Handwheel steer angle (HSA)
Root mean square (RMS)
Power Spectral Density (PSD)
Load transfer ratio (LTR)
Vertical tyre forces (VTFs)
Lateral Sideslip Limit (LSL)

References

[1] Vegvesen, SBJ-31-C3-MUL-22-RE-100 - Analysis and Design (Base Case) Bjørnafjorden, Straight Floating Bridge Phase 3 Analysis and Design (Base Case), 2017.

[2] B. Wang, Y.L. Xu, Safety analysis of a road vehicle passing by a bridge tower under crosswinds, J. Wind Eng. Ind. Aerod. 137 (2015) 25–36, https://doi.org/10.1016/j.jweia.2014.11.017.

[3] L.D. Zhu, L. Li, Y.L. Xu, Q. Zhu, Wind tunnel investigations of aerodynamic coefficients of road vehicles on bridge deck, J. Fluid Struct. 30 (2012) 35–50, https://doi.org/10.1016/j.jfluidstructs.2011.09.002.

[4] B. Wang, Y.L. Xu, L.D. Zhu, Y.L. Li, Crosswind effect studies on road vehicle passing by bridge tower using computational fluid dynamics, Eng. Appl. Comput. Fluid Mech. 8 (3) (2014) 330–344, https://doi.org/10.1080/19942060.2014.11015519.

[5] T. Argentini, E. Ozkan, D. Rocchi, A. Zasso, Cross-wind effects on a vehicle crossing the wake of a bridge pylon, J. Wind Eng. Ind. Aerod. 99 (2011) 734–740, https://doi.org/10.1016/j.jweia.2011.01.021.

[6] D. Sekulic, A. Vdovin, B. Jacobson, S. Sebben, S. Johannesen, Analysis of vehicles path tracking ability and lateral stability on a floating bridge under crosswind, J. Wind Eng. Ind. Aerod. 227 (2022) 105070, https://doi.org/10.1016/j.jweia.2022.105070.
[7] Y. Zhou, S. Chen, Vehicle ride comfort analysis with whole-body vibration on long-span bridges subjected to crosswind, J. Wind Eng. Ind. Aerod. 155 (2016) 126–140, https://doi.org/10.1016/j.jweia.2016.05.001.
[8] K. Nguyen, A. Camara, O. Rio, L. Sparowitz, Dynamic effects of turbulent crosswind on the serviceability state of vibrations of a slender arch bridge including wind–vehicle–bridge interaction, J. Bridge Eng. 22 (11) (2017) 06017005, https://doi.org/10.1061/(ASCE)BE.1943-5592.0001110.
[9] B. Jacobson, Vehicle Dynamics Compendium, Chalmers University of Technology, Gothenburg, Sweden, 2019. https://research.chalmers.se/publication/513850/file/513850_Fulltext.pdf. (Accessed 17 December 2023).
[10] X. Yang, J. Song, J. Gao, Fuzzy Logic based control of the lateral stability of tractor semitrailer vehicle, Math. Probl Eng. 16 (2015) 692912, https://doi.org/10.1155/2015/692912.
[11] D. Sekulic, V. Dedovic, S. Rusov, S. Salinic, A. Obradovic, Analysis of vibration effects on the comfort of intercity bus users by oscillatory model with ten degrees of freedom, Appl. Math. Model. 37 (18) (2013) 8629–8644, https://doi.org/10.1016/j.apm.2013.03.060.
[12] R.C. Lin, D. Cebon, D.J. Cole, Active roll control of articulated vehicles, Veh. Syst. Dyn. 26 (1) (1996) 17–43, https://doi.org/10.1080/00423119608969300.
[13] A.H. Jeyed, A. Ali Ghaffari, Development of a novel nonlinear estimator based on state-dependent Riccati equation technique for articulated vehicles, Proc IMechE Part K: J Multi-body Dynamics 233 (3) (2019) 516–530, https://doi.org/10.1177/1464419318811254.
[14] R. Nigam, Characteristics of Fifth Wheel and its Influence on Handling and Maneuvering of Articulated Heavy Vehicles, Chalmers University of Technology, Gothenburg, Sweden, 2018. https://odr.chalmers.se/items/e5477d8d-b35c-47c8-9f53-8903775653d6. (Accessed 7 January 2024).
[15] MSC, Software, Adams/Car Truck Help, Adams, USA, 2013.
[16] P. Sivaramakrishnana, A.K. Madhava Prakasha, D. Sekulic, B. Jacobson, C. Selvi, M.S. Johannesen, Methods to introduce floating bridge motion and wind excitation on a model for the investigation of heavy vehicle dynamics, Appl. Math. Model. 117 (2023) 118–141, https://doi.org/10.1016/j.apm.2022.11.038.
[17] V. Santahuhta, Roll Dynamics and Tyre Relaxation in Heavy Combination Vehicle Models for Transient Lateral Manoeuvres, Master Thesis in Vehicle Dynamics, Chalmers University of Technology, Gothenburg, Sweden, 2019.
[18] D. Sekulic, A. Vdovin, B. Jacobson, S. Sebben, M.S. Johannesen, Effects of wind loads and floating bridge motion on intercity bus lateral stability, J. Wind Eng. Ind. Aerod. 212 (2021) 104589, https://doi.org/10.1016/j.jweia.2021.104589.
[19] T.L. Phan, T.T. Nguyen, T.H.T. Nguyen, Optimization of unsteady jet control flow method for aerodynamic drag reduction of heavy truck model, Results, Eng. 22 (2024) 102167, https://doi.org/10.1016/j.rineng.2024.102167.
[20] C.R. Jadhav, R.P. Chorage, Modification in commercial bus model to overcome aerodynamic drag effect by using CFD analysis, Results, Eng 6 (2020) 100091, https://doi.org/10.1016/j.rineng.2019.100091.
[21] N. Chen, Y. Li, B. Wang, Y. Su, H. Xiang, Effects of wind barrier on the safety of vehicles driven on bridges, J. Wind Eng. Ind. Aerod. 143 (2015) 113–127, https://doi.org/10.1016/j.jweia.2015.04.021.
[22] L. Ma, D.J. Zhou, J. Wu, W.S. Han, J.X. Liu, Transient aerodynamic forces of a vehicle passing through a bridge tower's wake region in crosswind environment, Wind Struct. 22 (2) (2016) 211–234, https://doi.org/10.12989/was.2016.22.2.211.
[23] D. Sekulic, A. Vdovin, B. Jacobson, S. Sebben, S. Johannesen, Determination of safe speeds for a coach travelling on a floating bridge, Transp. Res. Interdiscip. Perspect. (2023) submitted for publication.
[24] F. Chen, S. Chen, Reliability-based assessment of vehicle safety in adverse driving conditions, Transp. Res. C: Emerg. Technol. 136 (4) (2011) 156–168, https://doi.org/10.1016/j.trc.2010.05.003.
[25] F. Chen, S. Chen, Simulation-based assessment of vehicle safety behavior under hazardous driving conditions, J. Transport. Eng. 19 (1) (2010) 304–315, https://doi.org/10.1061/(ASCE)TE.1943-5436.0000093.